# CFD Integrated Transition Modeling for High-Speed Flows via Coupled OVERFLOW-LASTRAC Analysis

Ethan A. Vogel* and Balaji Shankar Venkatachari† and Pedro Paredes‡
*National Institute of Aerospace, Hampton, VA 23666*

Fei Li§ and Meelan Choudhari¶
*NASA Langley Research Center, Hampton, VA, 23681*

**This work details ongoing efforts at the NASA Langley Research Center to develop and validate a general-use CFD tool that includes built-in predictions of boundary-layer transition in high-speed flows. Existing tools for the coupling of the NASA OVERFLOW structured overset RANS solver and LASTRAC stability analysis code have been extended to capture boundary-layer transition in high-speed flows driven by either Mack's first-mode or second-mode instabilities and/or crossflow instabilities. The efficacy of this coupled approach has been demonstrated by examining a variety of supersonic and hypersonic test cases for which experimental validation data is available. The intermittency prescription parameters inherited from prior low-speed applications are found to be suitable for some, but not all high-speed flow scenarios. The method is found to be robust for straight cone configurations and improvements necessary to accurately capture transition on geometries with spatially complex amplification factor envelopes with intermediate regions of slow N-factor variation are examined. The automated, coupled analysis is demonstrated for a 3d supersonic test case and found to perform well within the limits of the linear stability analysis on which it relies. Finally, a preliminary investigation of the method's robustness to non-ideal CFD meshes is conducted.**

## Nomenclature

| | | |
|---|---|---|
| $C_1$, $C_2$ | = | Coefficients for intermittency calculation |
| $f$ | = | Disturbance frequency [kHz] |
| $k$ | = | Intermittency length scaling factor |
| $P$ | = | Pressure [kPa] |
| $\mathbf{q}$ | = | Vector of flow variables |
| $\overline{\mathbf{q}}$ | = | Vector of mean flow variables |
| $\widetilde{\mathbf{q}}$ | = | Vector of perturbation flow variables |
| $\widehat{\mathbf{q}}$ | = | Vector of perturbation flow variables |
| $N$ | = | Logarithmic amplification factor |
| Re | = | Unit Reynolds number [$m^{-1}$] |
| $\mathrm{Re}_x$ | = | Local length-based Reynolds number [$m^{-1}$] |
| $r$ | = | Radial coordinate [m] |
| $t$ | = | Time [s] |
| $T$ | = | Temperature [K] |
| $x$ | = | Axial coordinate [m] |
| $y$ | = | Spanwise coordinate [m] |
| $\alpha$ | = | Streamwise wave number |
| $\beta$ | = | Spanwise wave number |
| $\gamma$ | = | Intermittency |

*Research Engineer, ethan.a.vogel@nasa.gov, AIAA Member
†Sr. Research Engineer, balaji.s.venkatachari@nasa.gov, Senior AIAA Member
‡Sr. Research Engineer, pedro.paredes@nasa.gov, Senior AIAA Member
§Aerospace Technologist, Computational AeroSciences Branch, fei.li@nasa.gov
¶Aerospace Technologist, Computational AeroSciences Branch, m.m.choudhari@nasa.gov, AIAA Fellow

| | | |
|---|---|---|
| $\nu$ | = | Underrelaxation factor |
| $\Xi$ | = | Nondimensional distance in transition region |
| $(\xi, \eta, \phi)$ | = | Body-fitted coordinates |
| $\rho$ | = | density [kg m$^{-3}$] |
| $\phi$ | = | Azimuthal angle [°] |
| $\omega$ | = | disturbance angular frequency [rad s$^{-3}$] |
| *subscripts* | | |
| $i$ | = | Corresponding to mode $i$ |
| $j$ | = | Corresponding to iteration $j$ |
| pred | = | Location where transition amplification factor is predicted |
| tr | = | Location where transition N factor is reached |
| x | = | Corresponding to given x location |
| 0 | = | Downstream extent of transition zone |
| 1 | = | Downstream extent of transition zone |
| $\infty$ | = | Freestream value |
| *subscripts* | | |
| + | = | defined in wall coordinates |

# I. Introduction

The CFD Vision 2030 identifies integrated prediction of laminar to turbulent transition within general purpose CFD codes as a critical and pacing item [1]. Prediction of laminar to turbulent transition is of critical importance in the design and evaluation of aerospace systems in all speed regimes. This is especially true for high-speed systems, where turbulent transition not only elevates the skin friction drag experienced by a vehicle, but also significantly increases the surface heat flux it experiences [2]. The state of the flow therefore partially dictates the necessary structure of the aerospace system and must be accounted for in the design phase of that system. For this to be possible, it is necessary to develop reliable, computationally affordable, user friendly, and robust means of predicting the transitional characteristics of high-speed flows.

For flows over smooth surfaces with sufficiently low levels of free-stream disturbances, transition is initiated by modal instabilities. The type of instability depends on the free-stream Mach number, vehicle shape, surface temperature, and the external disturbance environment. At low subsonic Mach numbers, planar Tollmien-Schlicting (TS) waves are dominant. Increasing the free-stream velocity leads to oblique first-mode instabilities taking a dominant role, and as velocity increases further to the hypersonic regime Mack-mode instabilities come into play [3]. Mack's second-mode instabilities are of chief interest here.

There are three general methods of predicting laminar-turbulent transition as part of an integrated, i.e., coupled prediction of an overall flowfield that includes laminar, transitional, and turbulent regions. In decreasing order of computational cost and complexity, these are scale-resolving simulations, stability analyses, and transport equation-based transition models. Scale-resolving simulations, such as those presented in Refs. [4] and [5] can reliably and robustly predict laminar-turbulent transition when sufficient information about the disturbance environment and/or the initial disturbance spectra in the boundary layer is available. However, the computational expense associated with the high-fidelity simulations precludes their use in design contexts. Moreover, this type of simulation often requires specialized software or tools, such as high-order, low-dissipation algorithms and synthetic turbulent inflow (described in Ref. [6]), to accurately replicate free-stream conditions for the prediction of transition. These techniques are not widely available in standard CFD solver distributions, and so are often not practical for those outside of the research community. Transport equation-based models, such as the commonly used Menter $\gamma$-Re$_{\Theta t}$ [7], Menter $\gamma$ [8], and Coder AFT [9] models, are widely used, but face fundamental issues related to their extension to high-speed flows. Transport equation models are constructed from experimental or scale-resolved simulation data and seek to replicate the salient characteristics of the flow configurations they are employed to study. This phenomenological approach is well-suited to analyzing systems that are sufficiently similar to the cases used to construct the model but is of lesser efficacy when the cases being studied include conditions or physical mechanisms outside of the original scope of the model. This issue has manifested in recent literature in the failure of widely used models for flow configurations at high Mach number [10], and also with particularly challenging low-speed cases as seen in Ref. [11]. In response to these shortcomings, various researchers have proposed new models or corrections to existing models that seek to address the issues with current popular techniques [12], [13]. Despite these recent gains, the formulation of transport equation models means

that there will always be some ambiguity in their predictions for novel configurations.

The intermediate methodology for transition modeling is the inclusion of semi-empirical transition correlations based on stability analysis about a mean flow [14]. A recent example of incorporating this approach in an unstructured flow solver is detailed in Ref. [15]. The most reliable approach for stability-based transition estimation corresponds to direct computations of linear stability based on the boundary-layer flow in the laminar regions(s). However, such analyses require a well-resolved mean flow to which the stability analysis will be applied. In a typical flow simulation, the resolution requirements for this mean flow are more restrictive than those for a transport equation model, but much less restrictive than even the least expensive scale-resolving simulations. Stability analyses are also physic-informed, and so the limitations of applicability often faced by transport equation models are less relevant in their context. At present, the largest barrier to adoption of stability analyses for transition prediction in general applications is a lack of sufficiently automated and robust stability analysis tools that can readily interface with existing production CFD codes and do not require the CFD user to be experienced in performing linear stability analysis. Because the stability analysis requires that a base flow be generated first, the stability calculation must be conducted as a separate, coupled computation from the Navier-Stokes solver.

There are examples in the literature of coupled stability predictions with the in-house CFD codes of ONERA and DLR [16–18]. Additionally, the works of Shi et al. [19] and Halila et al. [20] at the University of Michigan demonstrate the pursuit of adjoint-optimization. This work describes the state of ongoing efforts by the Computational AeroSciences Branch at the NASA Langley Research Center (LaRC) to develop and validate a coupled software suite for applications to high-speed transition problems using the NASA-developed Reynolds-averaged Navier Stokes (RANS) solver OVERFLOW and the LaRC stability analysis tool LASTRAC [21].

The work presented here is a continuation of ongoing efforts to couple LASTRAC to production CFD codes for general applications [15, 21]. Prior work has focused on subsonic flow scenarios. This work explores the extension of this coupled methodology to canonical supersonic and hypersonic flows. The remainder of this paper highlights the steps involved in this coupled approach and outlines the test cases used to mature and evaluate the method. The present work also identifies what future work will be pursued to continue developing this capability.

## II. Methodology

This section outlines the process by which the automated process computes transitional flow results in this work. First, a brief description of the constituent software packages and their functionality is provided. Next, the test cases analyzed in this work are outlined. Finally, the means by which the OVERFLOW CFD analysis is coupled to the LASTRAC stability calculation is described, with special attention paid to the aspects of the analysis unique to three-dimensional computations and the changes made specifically for high-speed flow scenarios.

### A. LASTRAC Stability Computations

LASTRAC is a flow stability analysis package developed and maintained by NASA Langley Research Center (LaRC) [22]. The software has been used extensively in the literature for stability calculations for hypersonic flow applications. LASTRAC is capable of performing linear stability theory (LST) and parabolized stability equations (PSE) analysis. This work principally uses it for LST computations.

LST computation is performed given an input mean flow which describes the basic state of the primitive flow quantities. This will be denoted here as $\mathbf{q}(\xi, \eta, \zeta, t) = (\rho, u, v, w, T)$. The state of the flow is considered to be the sum of a mean and time-varying state such that $\mathbf{q}(\xi, \eta, \zeta, t) = \overline{\mathbf{q}}(\eta) + \widetilde{\mathbf{q}}(\xi, \eta, \zeta, t)$. The perturbations about the mean flow, $\widetilde{\mathbf{q}}$, take the form

$$\widetilde{\mathbf{q}} = \widehat{\mathbf{q}} exp(i[\alpha\xi + \beta\zeta - \omega t]), \tag{1}$$

where the perturbations are assumed to be periodic in time and in the streamwise and spanwise directions. Equation. 1 can be substituted into the linearized Navier Stokes equations and solved as an eigenvalue problem. The growth rates of disturbances in LST are found as the imaginary part of the resulting eigenvalues, $\alpha$, as in

$$\sigma(\xi, \omega, \beta) = -\Im(\alpha). \tag{2}$$

A complete description of the linear stability computation can be found in Ref. [23]. The amplification ratio, often referred to as the N-factor, for a given $\beta$-$\omega$ combination is found as the integral of the growth rate over the streamwise distance from some upstream point. Ideally this is where the mode becomes unstable. This takes the form

$$N_i(\xi, \beta, \omega) = \int_{\xi_1}^{\xi} \sigma(\xi', \omega, \beta) d\xi', \tag{3}$$

and the amplification at a given point on the surface of the body in question is

$$N(\xi) = \max[N_i(\xi, \beta, \omega)]. \tag{4}$$

In practical stability computations, discrete increments of $\omega$ and $\beta$ are studied with the goal of adequately representing the continuum spectrum.

### B. OVERFLOW 2.3

The CFD tool used here is the NASA OVERFLOW 2.3e solver [24]. OVERFLOW is a structured overset RANS solver with multiple turbulence modeling options. Important for the coupled analysis is the OVERFLOW capability to impose an externally calculated intermittency. OVERFLOW is also capable of exporting specified subsets of the grid and solution from a computation, and of applying custom isothermal boundary conditions specified by a file. The ability to export domain subsets allows for computationally tractable subdomains to be exported for stability analysis. OVERFLOW-LASTRAC coupling has been established previously, and OVERFLOW's ability to perform high-speed flow computations enables the extension of this coupled transition prediction approach to higher Mach numbers.

### C. Test Cases

A number of test cases are employed in this work to develop and evaluate the coupled transition prediction methodology across a variety of high-speed flow conditions. Each test case examined is referenced to an experimental ground or flight test described in the literature so that the performance of the coupled prediction can be benchmarked. This suite of test cases is limited to canonical conical configurations. Future work is planned to evaluate the performance of the method in the presence of shockwave-boundary layer interactions, but the scope of this work is limited to maturing and evaluating the ability of the method to predict transition in smooth high-speed base flows, which is a prerequisite to studying more complex flows. The details of the different test cases examined in this work are described in this section and summarized in Table 1.

#### *1. HIFiRE-1*

The first set of test cases examined for this work are a selected set of trajectory points from the ascent phase of the HIFiRE-1 flight experiment [25]. This case has been studied in previous works, both in the context of the post-flight data analysis [26] and in the course of developing a deep-learning-based surrogate model for second-mode amplification [27].

This study examines the HIFiRE-1 flight experiment at times between $t = 19$ s and $t = 22$ s of the flight experiment in increments of 1 s. A fifth case from within this range is also examined for purposes of validating the base flow solution and developing the PyLASTRAC scripts. The HIFiRE-1 cone is a 7-degree half-angle cone that is 1.1 m long and has a nose radius of 2.5 mm. The freestream Mach number in this time domain ranges from 4.66 at the earliest time to 5.31 at the latest. The unit Reynolds number ranges from $2.058 \times 10^7$ m$^{-1}$ at $t = 19$ s to $1.147 \times 10^{7-1}$ at $t = 22$ s. The wall temperature is calculated as in Ref. [26] from experimentally-described heat flux. The free-stream temperature in each case is approximately 203 K.

For analysis corresponding to each time snapshot analyzed here, a different computational mesh was generated to ensure the grid was consistently shock-aligned. Each mesh was $607 \times 537$ in the streamwise and wall-normal directions, respectively. Wall spacings are chosen such that $y^+ = 0.1$ at the wall. Shock-aligned meshes are generated with a precursor run which was used to identify the profile of the shockwave and the boundary-layer edge. The exception to this was the $t = 21.5$ s case which was used for validation and script development purposes. This mesh was produced by the VULCAN-CFD shock adaptation routines in early analysis [26]. The transition value of the amplification factor, $N_{tr}$, for these cases is chosen to be 14.7, which is a representative transition N-factor based on Ref. [26].

#### *2. LaRC M6 Straight Cone*

The next test case examined here is the hypersonic straight cone (5dSCH) configuration examined in Ref. [28]. This configuration is a 5-degree cone without a flared section. The cone is 0.635 m (25 in.) long and the experimental model

**Table 1 Test Case Parameters**

| case | model | $M_\infty$ | Re ($m^{-1}$) | $T_\infty$ (K) | $T_{wall}$ (K) | $N_{tr}$ | Experimental Data |
|---|---|---|---|---|---|---|---|
| HF1 21.5 | HIFiRE-1 | 5.30 | 13.42e6 | 201.4 | Exp. Dist. | 14.7 | Kimmel et al. [25] |
| HF1 19 | HIFiRE-1 | 4.66 | 20.58e6 | 205.3 | Exp. Dist. | 14.7 | Kimmel et al. [25] |
| HF1 20 | HIFiRE-1 | 5.07 | 18.46e6 | 201.0 | Exp. Dist. | 14.7 | Kimmel et al. [25] |
| HF1 21 | HIFiRE-1 | 5.28 | 15.28e6 | 199.2 | Exp. Dist. | 14.7 | Kimmel et al. [25] |
| HF1 22 | HIFiRE-1 | 5.31 | 11.74e6 | 203.7 | Exp. Dist. | 14.7 | Kimmel et al. [25] |
| LaRC M6 | LaRC 5dSCH | 6.0 | 14.10e6 | 60.56 | 298.76 | 7.2 | Horvath et al. [28] |
| JAXA axisym | JAXA SC1 | 2.0 | 12.20e6 | 300 | 300 | 5.6 | Tokugawa et al. [29] |
| JAXA 3D | JAXA SC1 | 2.0 | 12.20e6 | 300 | 300 | 7.0 | Tokugawa et al. [29] |
| LaRC M3.5 A | LaRC 5dSCS | 3.5 | 28.10e6 | 92.22 | adiab. | 9.0 | Chen et al. [30] |
| LaRC M3.5 B | LaRC 5dSCS | 3.5 | 38.50e6 | 92.22 | adiab. | 9.0 | Chen et al. [30] |
| LaRC M3.5 C | LaRC 5dSCS | 3.5 | 49.00e6 | 92.22 | adiab. | 9.0 | Chen et al. [30] |
| LaRC M3.5 D | LaRC 5dSCS | 3.5 | 58.90e6 | 92.22 | adiab. | 9.0 | Chen et al. [30] |
| LaRC M3.5 F | LaRC 5dSCS | 3.5 | 78.00e6 | 92.22 | adiab. | 9.0 | Chen et al. [30] |

was designed with a replaceable nose tip to examine the influence of the nose radius on the stability characteristics of the flow. For this study, the sharp cone configuration is chosen for analysis, the nose radius was 0.00254 mm [28].

This case was run at conditions to match the NASA 20-inch Mach 6 wind tunnel experimental conditions. The free-stream $M_\infty = 6.0$, $T_\infty = 61.11$ K, and a variety of unit Reynolds numbers. These cases were run with a wall temperature of 300 K. The computational mesh was $759 \times 537$ in the streamwise and wall-normal directions respectively.

*3. JAXA SC1 Cone*

The JAXA straight cone 1 (SC1) configuration was chosen to extend the coupled solver methodology to Mack's first-mode instabilities and stationary crossflow instabilities. The SC1 is a 5° straight cone with a nose radius of 4 $\mu$m and a length of 0.3 m. The configuration was first analyzed in Ref [29] and is examined here both as an axisymmetric simulation with zero angle of attack and as a three-dimensional simulation with an angle of attack of 2°. For both cases, shock-aligned grids derived from VULCAN-CFD calculations were used for the OVERFLOW-LASTRAC analysis. This case was run at conditions that replicate the Fuji Heavy Industries Mach 2 tunnel conditions. The free-stream conditions are $M_\infty = 2.0$, $T_\infty = 165$ K, and $Re_\infty = 12.2 \times 10^6$ $m^{-1}$. These cases were run with a wall temperature of 300 K. The axisymmetric grid is $577 \times 513$ in the streamwise and wall-normal directions respectively, and the 3D grid is $609 \times 257 \times 577$ in the streamwise, spanwise, and wall-normal directions, respectively.

*4. LaRC Supersonic Cone*

The LaRC supersonic cone configuration (5dSCS) was analyzed by Chen et al. [30] in the NASA Langley Mach 3 Pilot Low-Disturbance Tunnel. The model is a 5° half-angle cone with an axial length of 0.381 m and a nose radius of 0.025 mm. This test case is primarily for the tuning and evaluation of the first-mode transition prediction scripts. In this work, five of the runs reported in Ref. [30] are analyzed. The freestream unit Reynolds numbers for the selected cases are $7.80 \times 10^7$ $m^{-1}$, $5.89 \times 10^7$ $m^{-1}$, $3.85 \times 10^7$ $m^{-1}$, and $2.81 \times 10^7$ $m^{-1}$. For all of these cases, $M_\infty = 2.0$ and $T_\infty = 92.22$ K.

Meshes for this family of cases are composed of $577 \times 513$ points in the streamwise and wall-normal directions, respectively. Ref [30] estimate the critical N-factor for each of these cases to be close to 10, and Ref. [31] found that N-factors between 9 and 11 were associated with transition in this case. For this work it was found that an N-factor of 9 produced reasonable results, and like the HIFiRE test cases it was desirable to use a single characteristic N-factor so analysis could focus first on transition region length.

For this study all meshes are shock-aligned and boundary-layer refined. While not strictly necessary for calculating the solution, shock-alignment improves the quality of the results from stability analysis calculated from the base flow.

### D. RANS Solution Parameters

Stability analysis has stricter requirements on mean-flow accuracy than the estimation of conventional metrics related to force and moment characteristics and integrated heat flux. For purposes of stability analysis, it is often necessary to include a large number of points inside the boundary-layer, with a particular emphasis on resolving both the near wall region and the critical layer of the instability waves that is located in the outer part of the boundary layer. Typical grid-generation routines based on wall-normal marching with a specified initial wall spacing and growth rate tend to produce grids where the number of points in the simulated boundary layer increases with downstream distance. Grids for this simulation were therefore generated from an initial mesh which was used to identify the boundary-layer edge and shockwave location. The final mesh for each case was shock-aligned and boundary layer fitted with the goal of clustering sufficient points near the boundary-layer edge to facilitate stability analysis. Each case was initialized with a low Mach number preconditioning case, in which all of the grid and simulation parameters are identical except for the free-stream Mach number. Because the location of the shock depends on the Mach number, the shock-aligned mesh was marched an additional 50 points into the free-stream to aid with the convergence of this step. For cases with a spatially varying wall temperature, the wall temperature is imposed using OVERFLOW's native capabilities and read from an external file. For the HIFiRE-1 cases the initial transition location was chosen to be different in each case to verify that the workflow is robust with respect to initial assumed transition location. After this was verified, the initial simulation for each case was run with transition imposed via a trip line at a point just upstream of the end of the viscous domain.

All OVERFLOW solutions examined here used the HLLE++ upwind flux scheme, SSOR, and the van Albada limiter with added smoothing. Turbulent regions are simulated with the SA-neg turbulence model [32] with the exception of the LaRC Mach 6 cone data presented by Horvath et al [28], which used the SST turbulence model [33]. The preliminary run was used to evaluate the number of time steps required for convergence of the RANS run. The convergence history of a sample coupled calculation is presented in Fig. 1, where each color corresponds to a new iteration of the coupled process and the resudual is calculated as the $L^2$ norm right-hand side of the flow equations.

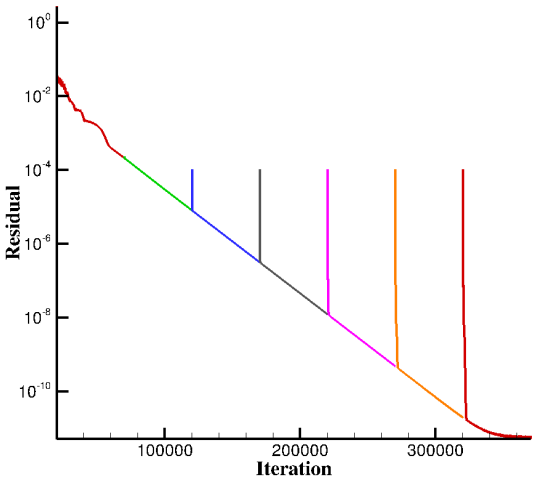


**Fig. 1 RANS residual, defined as the $L^2$ norm of the right-hand side terms of a sample HIFiRE-1 anlysis set at conditions corresponding to t = 19 s.**

### E. Coupled Solver Methodology

LASTRAC stability calculations are coupled to the OVERFLOW solver through external scripts written primarily in Python. A description of initial version of the PyLASTRAC software suite is may be found in [34]. Significant revisions to that capability were made as part of coupling those scripts to CFD solvers [15, 21] and in the course of the present work to extend them to high-speed flows. Before stability calculations can be performed, the OVERFLOW solution is extracted and converted to a plot3d-format function file. This extraction also trims the inviscid region from the domain that will be used for the stability analysis. This plot3d function file is then passed to a secondary

routine that converts the structured solution to an unstructured Tecplot formatted file. This step allows for the use of previously-validated automated routines for unstructured flows [15] to calculate streamlines along which the LASTRAC analysis will be applied and convert these subsets of the flow to LASTRAC data format. Python routines then perform an initialization set of LASTRAC linear stability analyses which scan for and identify the range of frequencies and/or wavelengths of interest. The parameters for this search are based on the type of instability the user identifies as of interest. Previous studies have demonstrated the progress of the constituent pieces of the PyLASTRAC suite to robustly predict Tollmien-Schlichting and crossflow transition. Here, we assess and improve upon the robustness of the software suite for Mack's second-mode instabilities. Once the range of frequencies and the physical domain of interest have been identified, the Python script automatically generate LASTRAC input files and executes the linear parabolized stability equations (PSE) or quasiparallel, linear stability theory (LST) analysis. The PyLASTRAC routines then extract an N-factor envelope from the output of the stability analysis. The envelope N-factor corresponds to the logarithmic amplification ratio of the most amplified mode at each given point in space. With this information, a final routine reads a surface grid file and identifies the grid position where the user-prescribed critical N-factor is reached. In addition to identifying the station $x_{tr}$ where $N = N_{tr}$, this routine also identifies $x_1$ where $N = C_1 N_{tr}$ and $x_2$ where $N = C_2 N_{tr}$. Here, the constants $C_1$ and $C_2$ are chosen based on available reference data. The default value of these parameters, which was chosen in previous studies for subsonic applications [21], are 0.8 and 1.1 respectively. One goal of the present work is to calibrate these parameters for high-speed applications. In updating the transition location, an under-relaxation factor of 0.7 is used. This is intended to aid the convergence cases where viscous-inviscid interaction leads to differences in the N-factor curves between successive simulations, and oscillations of the transition location between updates may occur. Next, an intermittency field for the RANS solver is defined by using the Gaussian distribution given by

$$\gamma = 1 - exp(-k\Xi^2), \tag{5}$$

where

$$\Xi = \frac{x - x(N = C_1 N_{tr})}{x(N = C_2 N_{tr}) - x(N = C_1 N_{tr})}. \tag{6}$$

In this equation, $k$ is a user-specified parameter which, along with the chosen value of $C_1$ and $C_2$, govern the width of the transition region. The baseline value of $k = 0.412$ was chosen in previous studies [21] based on calibration from low-speed flat-plate data as with the other intermittency constants. This work examines other values of $k$, $C_1$ and $C_2$ for high-speed flows, but identifying the correct value of $N_{tr}$, which also influences transition region width through coupling with the other parameters, is left to future work. With the intermittency calculated, a plot3d-format intermittency file is written and used during the next RANS calculation as input data that the OVERFLOW solver is able to use in computing the mean flow. The resulting flow solution is then used as the input for the stability analysis, and this cycle is repeated a user-specified number of times. For cases where the current transition location is upstream of the actual transition location, and so the value of $N$ never reaches $N_{tr}$, the transition location is predicted via linear extrapolation from the available laminar region.

For the cases examined here, $N_{tr}$ (for cases where it was not available from the reference data) was determined via a precursor laminar run and stability analysis. LST was used to calculate the amplification factor profile for the laminar base flow, and then this amplification profile was cross-referenced with the experimental transition location to determine $N_{tr}$. While this approach does not consider potential viscous-inviscid interactions that could alter the amplification profile as compared to the laminar base state, it is widely accepted in the literature and, indeed, the method used by Refs. [28–30] when $N_{tr}$ is provided. The authors acknowledge that the prediction of $N_{tr}$ from available facility characterization data and the mean flow input parameters is a necessary aspect of the coupled solver methodology being discussed. This aspect of the analysis is not included in this work, and future work is planned that will focus specifically on the determination of $N_{tr}$ for high-speed flows.

*1. Updates to Coupled Analysis*

While a number of changes and additions to the workflow were required for the 3D analysis, the underlying logic is largely preserved from the axisymmetric cases. Streamlines for stability computations were generated from seed points subsampled from the computational surface mesh. In its present form, the software tools that convert the plot3d-format grid and solution files to LASTRAC format, have a limit on the maximum file size that is violated by the JAXA-3D computational mesh. To make the analysis possible, the mesh was subsampled in the streamwise direction, and the subsampled grid and solution were used for stability calculations. The potential impact of this subsampling on the solution is explored in the results of this work.

Once streamlines are extracted, stability analysis is performed with automated scripts from the PyLASTRAC library that scan for and then examine unstable traveling crossflow modes. The result of this analysis is a set of streamlines defined along the body surface and N-factor profiles for each identified mode along that streamline. To create an N-factor envelope, the maximum N factor at each point along each streamline is identified with python tools. An example of the output of this process is shown in Fig.2.

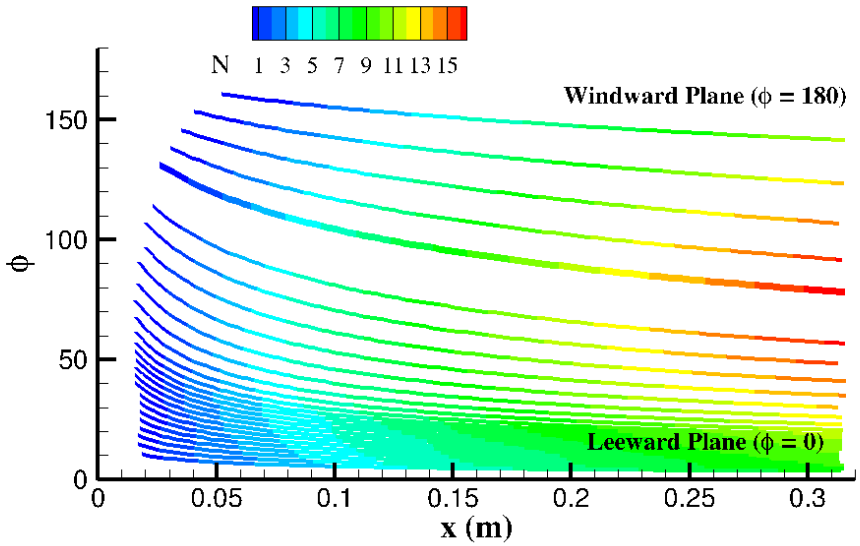


**Fig. 2 Demonstration of the streamline output of the 3D stability computation for the JAXA-3D case. The bolded streamline corresponds to the path used for comparison to previously-published analysis.**

Once an N-factor envelope for each streamline is found, Eqns. 5 and 6 are applied to the streamline to calculate a smooth intermittency distribution. These streamline-defined intermittency distributions are then interpolated onto the surface Tecplot file used in the stability computations and then onto the plot3d-format grid. This interpolation is performed in Tecplot 360, which allows for automation of the process via macro scripting. Future work will develop a python tool to perform this interpolation to reduce the number of additional tools required to use the coupled methodology. Creation of an in-house tool for this step of the process will also allow for smoothing of the N-factor envelopes to be performed at that step to remove the scalloping sometimes observed in discrete spectra calculations.

Once the intermittency distribution for the new iteration has been calculated, the new imposed value of intermittency at each grid point is found from the current and calculated distributions using the underrelaxation factor according to

$$\gamma = \nu\gamma_j + (1-\nu)\gamma_{j-1}. \tag{7}$$

For the three-dimensional case, no assumption of initial transition location is made. Instead, the first RANS simulation is configured to compute a fully laminar flow and no relaxation is applied in the first intermittency update. Equation 7 is only applied starting after the second CFD computation when the initial $\gamma$ distribution and from the laminar flow and the $\gamma$ distribution from the subsequent simulation are both available. This approach has qualitatively been found to accelerate the coupled solver approach by eliminating lag in the first few $\gamma$ updates for cases where there is not significant influence of viscous-inviscid interaction modifying the transition location and will be adopted to the axisymmetric cases in the future.

While many of the PyLASTRAC scripts used in the automated analysis for this work were already available from previous work, some of them required slight modification to increase their robustness to be able to calculate N-factor envelopes reliably for all relevant test cases here. For the second-mode computation, this amounted to slightly modifying

the frequency search parameters to expand the frequency range that the automated script would analyze. For the first-mode calculations, a new routine was developed, which combined elements of the existing tools.

This script is tuned to expand the search region to lower frequencies than the original second-mode script and to scan for oblique modes rather than planar modes. It is modified to scan a specified range of nondimensional azimuthal wave numbers ($\beta$) for axisymmetric cases. For these cases, beta is defined as $\beta = nl/r_b$ where $n$ is the wavenumber, $l$ is the flow length case, and $r_b$ is the local azimuthal radius. The crossflow analysis script used here is created by modifying the stationary crossflow script to scan for frequency and analyze a range of nondimensional azimuthal wavenumber. These scripts have been written for conical geometries like those analyzed here, and further development is required for extension to cases where the geometry in question is not axisymmetric and so this definition of $\beta$ is inappropriate.

### F. Intermittency Parameter Analysis

Three parameters govern the intermittency distribution along the streamline output by the automated routines as described in 5. Two of these parameters, $C_1$ and $C_2$, govern the width around the transition location where intermittency between 0 and 1 is imposed. The final parameter, $k$, dictates the slope of the Gaussian function imposed. Initially, values of 0.8, 1.1, and 0.412 were used for these three parameters. These parameters were found to produce good results for low-speed cases [21]. In the development of the coupled methods, an examination of these parameters for compressible flows is necessary.

Tuning of these parameters for the $2^{nd}$-mode cases was based on the Stanton number distribution for the HiFIRE-1 flight test experiment case. While multiple criteria for correlation efficacy could be chosen, heat transfer prediction is a first-order design driver for hypersonic systems and experimental Stanton number data are available. Tuning took an iterative approach where three of the HiFIRE-1 test cases for which data are available were analyzed with a sweep of PyLASTRAC versions set to use different intermittency parameters from a predetermined test matrix. The quality of the prediction was evaluated by comparing the width of the transition region predicted by each computation (in terms of the local length-based Reynolds number, $\mathrm{Re}_x$) to that found by the experiment.

Because the experimental transition was monitored with discrete thermocouples, it was necessary to interpolate between the available data points to develop an estimation of the transition region width. Each experimental result was curve fit by hand with a Gaussian function that approximated the size of the transition region, taking into account the expected shape of the transition front curve for cases such as $t = 20s$ where the experimental data points appear to include some noise or error. For the $t = 20s$ case, the upstream edge of the transition region could not be precisely located, and so the curve fit was created such that the transition region fell downstream of the farthest thermocouple at which the flow was laminar, but not so far downstream as to perfectly pass though the experimental heat flux value at the next thermocouple. The result is an intermediate value of the possible heat transfer profiles that could satisfy the experimental data within its error bars. The function used to estimate the transition width of the HIFiRE-1 case is shown in Fig. 3.

The first mode tuning was performed using a subset of the LaRC Mach 3.5 straight cone cases. The experimental recovery factor data for this case are more densely clustered than the HIFiRE data. The challenge in developing the curve fit to continually-define the recovery factor was in characterizing the overshoot region and, for the Re = 2.85e6 $\mathrm{m}^{-1}$ case, in identifying the appropriate upstream extent of the transition region given the experimental data. The function used to estimate the transition width of the M3SC case is shown in Fig. 4.

For both cases, the reference and computed transition width is found by calculating the axial distance (in units matching the experimental reference) between the upstream and downstream end of the transition region with a 5% buffer on either side. This buffer was based on the heat transfer or recovery factor difference between the upper and lower extent of the transition region to ensure a consistent metric between cases. For the HIFiRE-1 case, the upper and lower extent of the transition region was found by identifying the relative minimum in heat transfer at the start of transition and the relative maximum at the end of the transition region. Applying the 5% buffer to both the computed data allowed for a fair comparison between the two and the ascertainment of a relative error between the experiment and computation. For the SC1 case, this method needed to be adjusted because there is no relative maximum or minimum an automated analysis routine can use to identify the transition region. However, the recovery factor does have a consistent laminar and turbulent value, and analysis of results from four sets of intermittency parameters found that the computations in this analysis reliably converge to the same value on either side of the transition region. On the turbulent side, the value is approximately 0.884, and on the laminar side it was a value between 0.842 and 0.846, which varied based on Reynolds number but is consistent for a given Reynolds number to within approximately 0.001. This small variance appeared to be the result of small shifts in the transition location based on the tuning parameters. These values, with the appropriate

buffer applied, were used to identify the upper and lower extent of the transition region. Similar logic was applied to the experimental curve fit, using the upper and lower plateau values as the boundaries to which the 5% buffer is applied. For instances where the threshold value lay between grid points, linear interpolation was used to estimate its streamwise location.

Identification of the improved intermittency parameters for both cases took a brute force approach, where a discrete envelope of parameters was identified, and all possible combinations of parameters were tested. The best-performing combination was identified, and a new, more focused envelope was examined in the neighborhood of the best-performing parameters. This analysis does not consider transition location when evaluating error. Error was taken to be the average of the error of each of the three test cases examined for the mode type. Therefore, this analysis does not necessarily identify the parameters that perfectly replicate the transition profile of one test case, but the parameters that do the best overall job for all three.

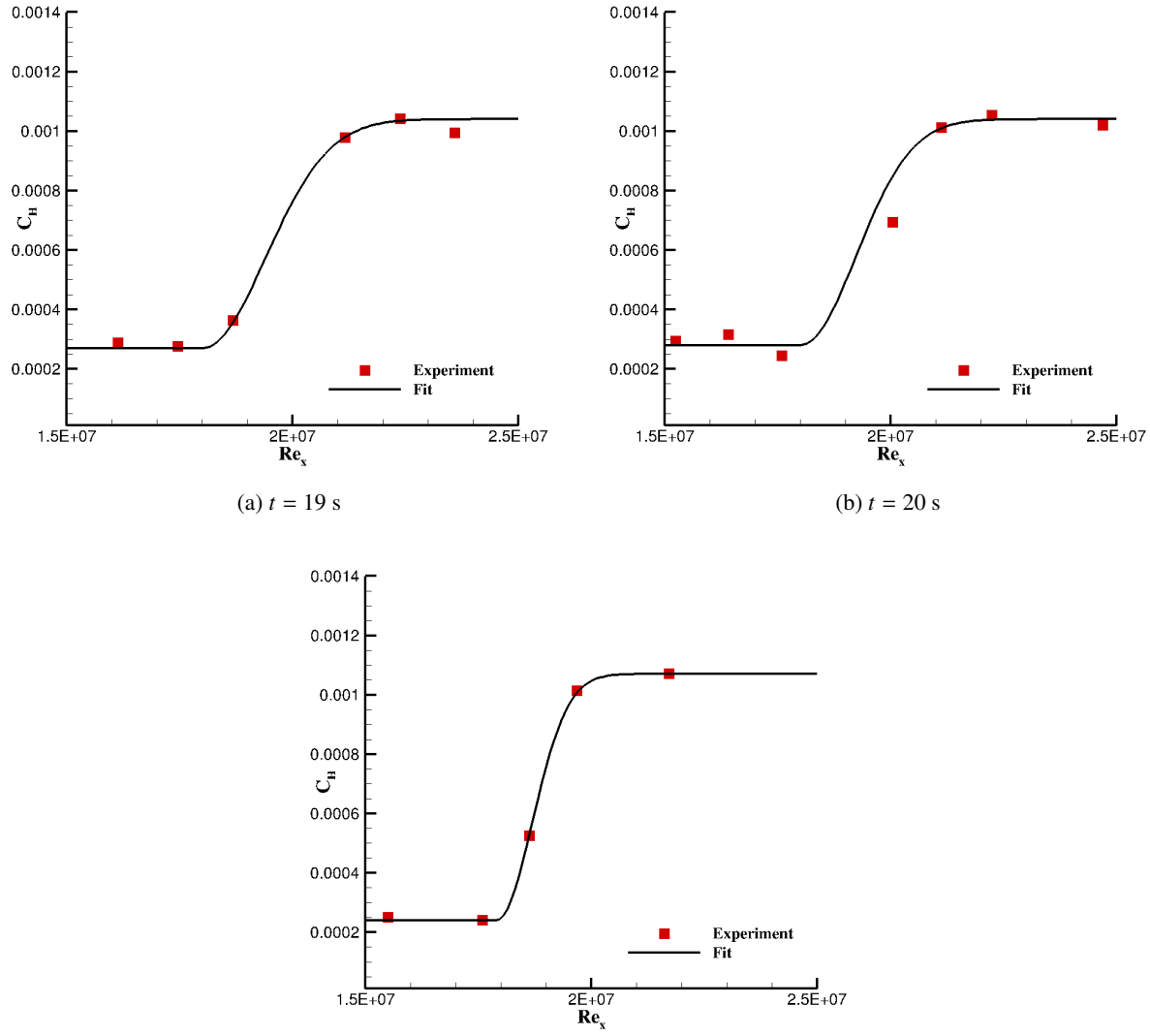


(a) $t$ = 19 s

(b) $t$ = 20 s

(c) $t$ = 21 s

**Fig. 3 Curve fits used to estimate the transition region width for the HIFiRE-1 test cases.**

One important caveat which must be made in the tuning of these parameters is that the analysis of $C_1$, $C_2$, and $k$ does not consider the location of the transition region, only its streamwise extent. Because, as discussed in section II.C, the HiFIRE-1 and LaRC Mach 3.5 cone analysis is performed using a single representative N factor to identify the

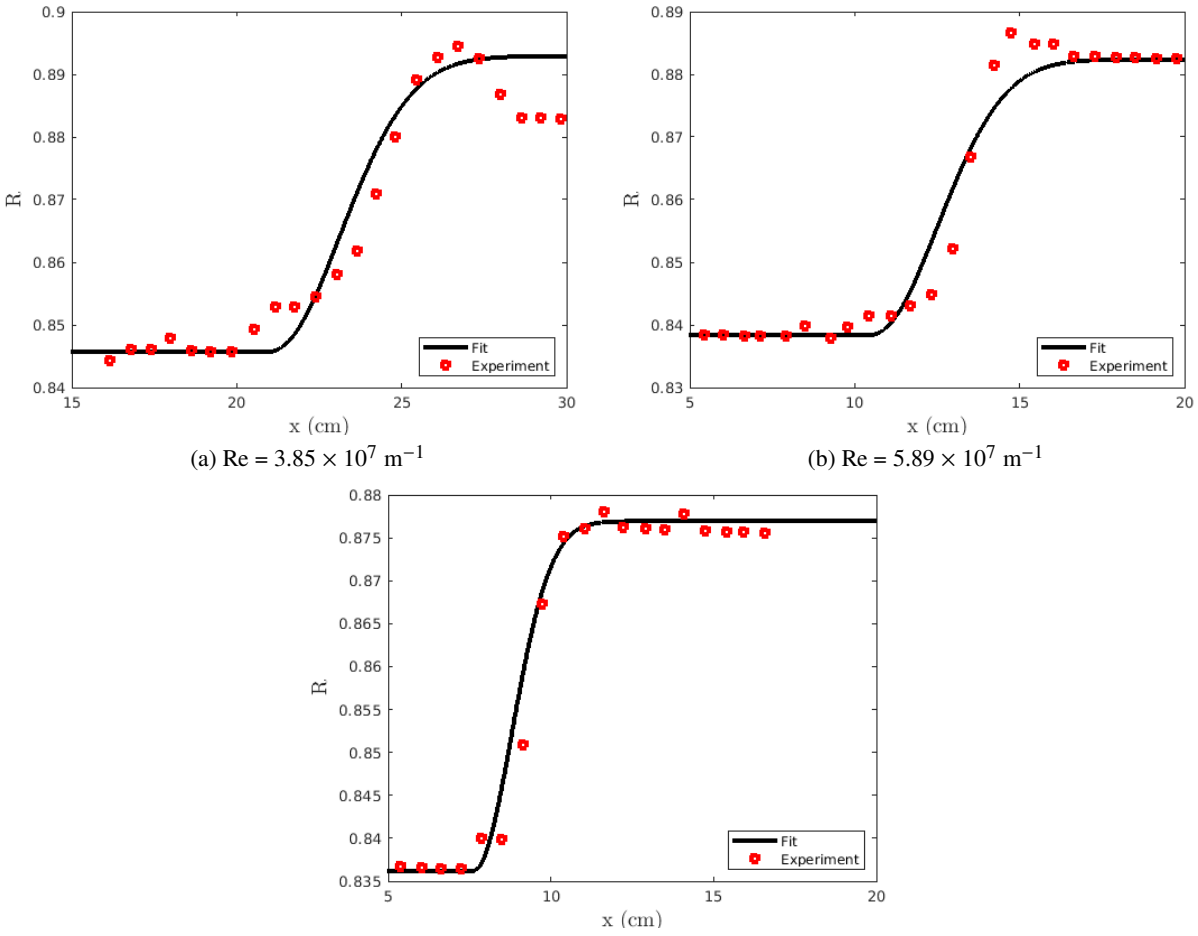


(a) Re = $3.85 \times 10^7$ m$^{-1}$

(b) Re = $5.89 \times 10^7$ m$^{-1}$

(c) Re = $7.80 \times 10^7$ m$^{-1}$

**Fig. 4 Curve fits used to estimate the transition region width for the Chen et al [30] cases.**

onset of transition, it is expected that the transition location will also be a source of some error in these calculations. This is because a single N factor is not fully descriptive of the transition amplification factor across all three different free-stream conditions. This approach hypothesizes that transition location and transition region length are sufficiently decoupled that each can be tuned separately. The development of a correlation for transition N factor is planned for future work and will begin by exploring a correlation analogous to Mack's correlation for low speeds [3]. In the literature, correlations between tunnel noise level and equivalent turbulence intensity have already been employed for transport model transition prediction [35]. These correlations may serve as a starting point for such an analysis, and the development of a satisfactory correlation may require advancement in the community's understanding of the receptivity mechanisms in high-speed flow that dictate the disturbance environment at the beginning of the modal growth region modeled here.

## III. Evaluation of Present Methods

Before the coupled analysis can be used to make transition predictions, confidence in the ability of the automated scripts to generate accurate LST results must be established. This section outlines the application of the coupled analysis by examining a single test case in detail, then compares the results of the present analysis to the validation test cases for which the original reference data are available.

### A. Illustration of Iteratively Coupled Process

This section demonstrates the workflow and functionality of the OVERFLOW-LASTRAC coupled analysis using the HIFiRE-1 case at t = 21.5 s as an example. This case was used to verify the $2^{nd}$-mode coupled analysis, and the trends observed with this case in this section are representative of those found for other test cases in this work. The Mach number contours near the nose of the cone are shown in Fig. 5, which shows the mean flow solution obtained during the final iteration. Because the flow does not contain shock-wave/boundary-layer interactions, the transition location does not have a strong influence on the flow outside of the boundary layer, and so this figure is sufficiently representative of all the RANS simulations conducted during the iterative analysis of the cases analyzed here. the evolution of the N-factor is shown in Fig. 6. For these cases, the N factor is found to abruptly drop to zero when the flow reaches the turbulent region and so that region has been removed from the N factor plots for clarity.

As shown in Table 2 the underrelaxation employed here slows the convergence of the solution to some extent. In this table, $x_{pred}$ is the transition location, $x_{tr}$, calculated by the code before the underrelaxation is applied. Convergence of the surface vorticity profiles and intermittency distributions across five iterations is shown in Fig. 7. While the robustness provided by the under relaxation is necessary for more complex configurations, a faster convergence can be achieved by making this parameter closer to unity in simple cases such as the HIFiRE-1 cone. For future works, the coupled methodology has been adapted so that the relaxation factor is not applied to the first iteration of the coupled transition location prediction. This will prevent the lag observed in this test case while maintaining the robustness the underrelaxation factor was introduced for. The stability results shown here correspond to disturbance frequencies within the interval of 210-900 kHz with an increment of 10 kHz.

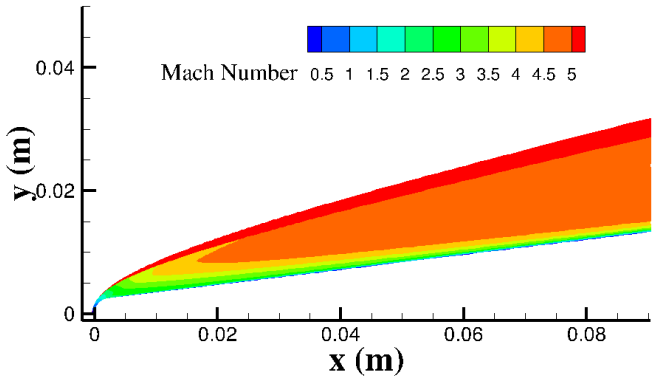


**Fig. 5 Mach number contours over the front part of the HIFiRE cone, based on the final iteration of the coupled process**

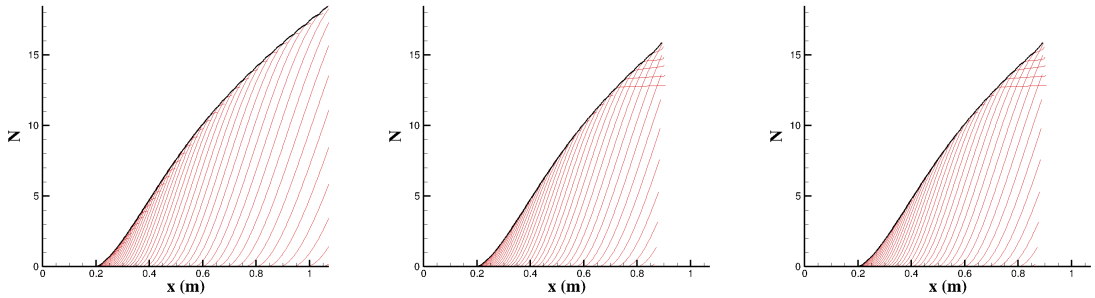


(a) Initial run (b) Second run (c) Third run

**Fig. 6 N-Factor curves for selected frequencies (red curves) and the corresponding envelopes (black curves) from the stability calculations performed for the first three iterations of the coupled process for HIFiRE-1 at t=21.5. Results are shown for frequencies between 210-900 kHz in increments of 10 kHz.**

**Table 2 Transition locations for each iteration**

| Iteration index | $x_{onset}$ | $x_{tran}$ | $x_{turb}$ | $x_{pred}$ |
|---|---|---|---|---|
| 1 | 1.000000 | 1.000000 | 1.000000 | - |
| 2 | 0.726252 | 0.880900 | 0.968100 | 0.829857 |
| 3 | 0.689954 | 0.845188 | 0.913973 | 0.829883 |
| 4 | 0.674241 | 0.834747 | 0.903260 | 0.829883 |
| 5 | 0.674649 | 0.829892 | 0.898669 | 0.829883 |
| 6 | 0.674648 | 0.829883 | 0.898667 | 0.829883 |
| 7 | 0.674648 | 0.829883 | 0.898667 | 0.829883 |
| 8 | 0.674648 | 0.829883 | 0.898667 | 0.829883 |

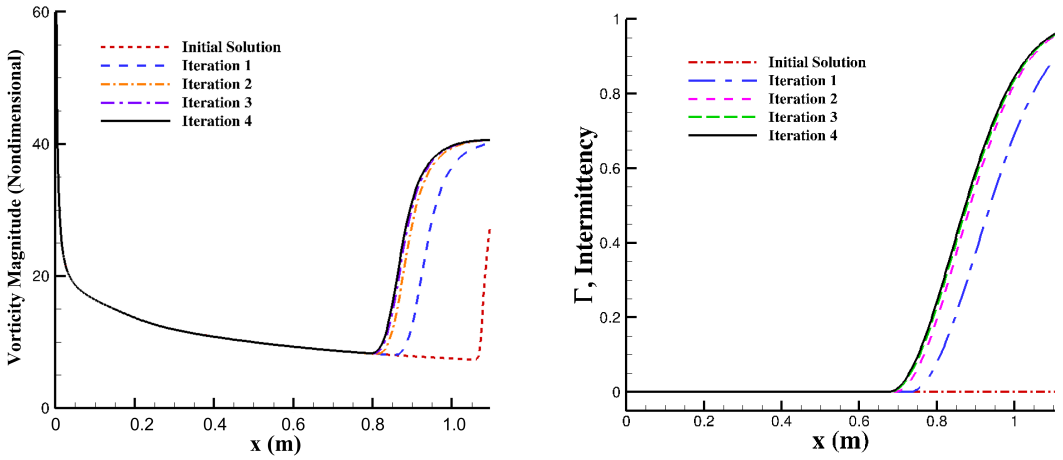


(a) surface vorticity magnitude.

(b) intermittency Profiles.

**Fig. 7 Convergence of the nondimensional vorticity magnitude at the surface and intermittency distribution for the first four iterations of the HF1 21.5 test case.**

The test case presented here specifies the initial transition location to be downstream of the known experimental transition location. Because of this, the N factor envelope is reliably able to reach $N_{tr}$, and the transition front advances upstream with each iteration of the coupled analysis until it reaches the correct position. To evaluate the robustness of the methodology, the HIFiRE test cases were also examined with initial transition locations substantially upstream of the experimental value. In all cases examined, the coupled analysis routine successfully converged to the correct value. For cases where the initial transition prediction was upstream of the actual value, the coupled routines estimate its location via extrapolation from the available N factor envelope. If this extrapolation did not yield a predicted transition location within the domain, then the transition location was updated to be halfway between the previously imposed transition location and the downstream boundary of the domain.

The intermittency and vorticity magnitude distributions at the end of the final iteration of this demonstration case are shown in Fig. 8. For this case, transition does not begin to occur until the intermittency parameter has risen to approximately 0.25. This tendency of the transition front to not exactly correspond to the imposed intermittency region is found in other test cases as well, and in some cases, transition does not begin until $\gamma$ is larger. In selected test cases, this is found to shift the transition onset downstream of the $x_{tr}$ location identified via the N factor envelope. This is an active area of continuing inquiry for the coupled analysis. With the coupled analysis process demonstrated in detail for a single test case, the remainder of this section is devoted to demonstrating the results obtained by it for several test cases and evaluating the advantages and challenges of the method.

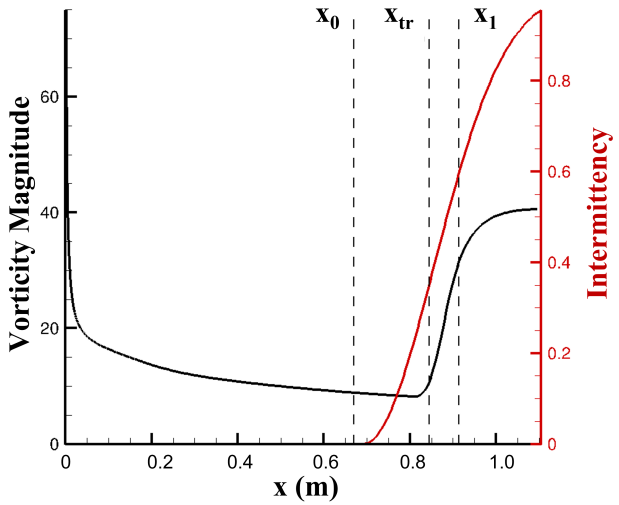


**Fig. 8 Axial distribution of intermittency and surface vorticity magnitude based on the third iteration of the mean flow calculation. The vertical dashed lines from left to right correspond to $x_1$, $x_{tr}$, and $x_2$, respectively.**

### B. Verification of OVERFLOW 2.3 Mean Flows

Prior stability analyses of structured-grid CFD solutions at LaRC has utilized solutions calculated from VULCAN-CFD, and the stability analysis included in the coupled methodology here is validated against those results. As such, it is necessary to demonstrate agreement in the base flow calculations provided by these two CFD solvers. In order to validate the CFD and stability calculations performed via OVERFLOW, base flow profiles from the HIFiRE-1 and JAXA cone are directly compared. Additionally, LASTRAC stability analyses for these cases were also performed with prescribed frequency and wave number inputs so the stability characteristics of both base flows could be directly compared.

For this comparison, the OVERFLOW base flow is calculated using a mesh adapted directly from the original VULCAN runs. The cases used for the validation of the base flows were the HIFiRE-1 case at t = 21.5 s, the JAXA SC1 cone at 0° angle-of-attack studied with an axisymmetric mesh, and the JAXA SC1 cone at 2° angle-of-attack studied with a three-dimensional mesh. Comparisons of the VULCAN to OVERFLOW data for the HIFiRE-1 case is shown in Fig. 9 and the comparison for the axisymmetric JAXA SC1 case is shown in Fig. 10. For the 3D case, profiles are extracted along the windward and leeward planes, as well as one intermediate plane, which is at an azimuthal position approximately 2/3 of the way between the windward and leeward planes. These comparisons are shown in Figs. 11, 12, and 13.

From these figures, it is clear that the OVERFLOW CFD agrees well with the Vulcan solutions calculated in previous studies. While both OVERFLOW 2.3 and Vulcan-CFD are widely used and validated CFD solvers, the confirmation of the agreement between the OVERFLOW and Vulcan base flows is a prerequisite for direct comparison of linear stability analysis results calculated from each.

### C. Evaluation of Automated LST Analysis

Robust transition prediction via coupled CFD-LST analysis requires that at all steps of the automated process reliably produce high-quality results. Previously, a major hurdle to the use of stability-based analysis for transition prediction has been the level of expertise required to reliably utilize the method. In substituting an automated routine for an experienced LST practitioner, it is necessary to confirm that the automated analysis produces the same results as would be found by an experienced human user, and to identify the source of any disagreements that are found. The three test cases used in the evaluation of the OVERFLOW basic state solutions are also used in the evaluation of the automated stability analysis.

Figure 14 compares the automatically-calculated N-factor envelope to the previously published results for the HF1 21.5 [26] case and the JAXA SC1 axisymmetric case [29]. For both of these cases, these results show good agreement between the automated and manual analysis.

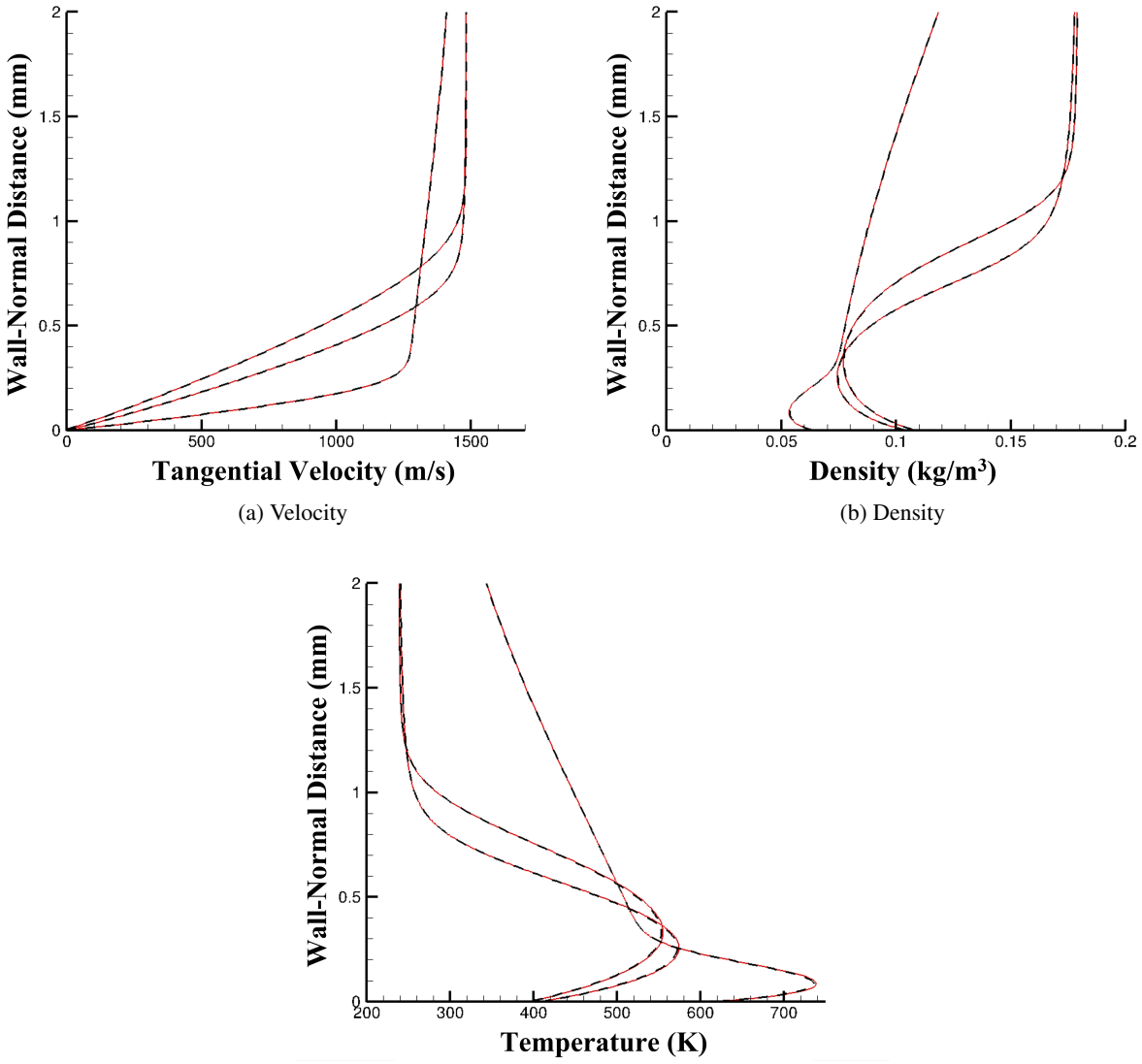


(a) Velocity

(b) Density

(c) Temperature

**Fig. 9 Comparison of mean flow profiles between OVEFLOW and VULCAN-CFD solutions at $\frac{x}{L}$ = 0.05, 0.5, and 0.8 for the HF1 21.5 case.**

Figure 15 shows the comparison between the N-factor profiles of selected modes for the 3D case near the windward and leeward plane. LASTRAC analysis is restricted to the interior of the domain, and so the streamline for this comparison in the unstructured, OVERFLOW-calculated base flow that is calculated using a seed point very near, but not at, the domain edge. Selection of a seed point for streamline calculations was found to be especially sensitive when analyzing the leeward plane of the flow where crossflow tended to push the streamline toward the domain edge as it propagated downstream. The automated analysis presented in section V.C was performed before this was learned, and automated analysis that incorporates more advanced streamline seeding techniques to ensure stability characteristics near the domain boundaries are captured is ongoing at the time of writing. As the figure shows, the windward and leeward planes show good agreement between the modes that make up the N factor envelope for both cases, though differences in the predictions are found in the modes interior to the envelope.

The intermediate streamline, chosen to pass through the region of the cone on that traveling crossflow instabilities are most amplified and highlighted in the presentation of the coupled results, presented some challenges in this analysis.

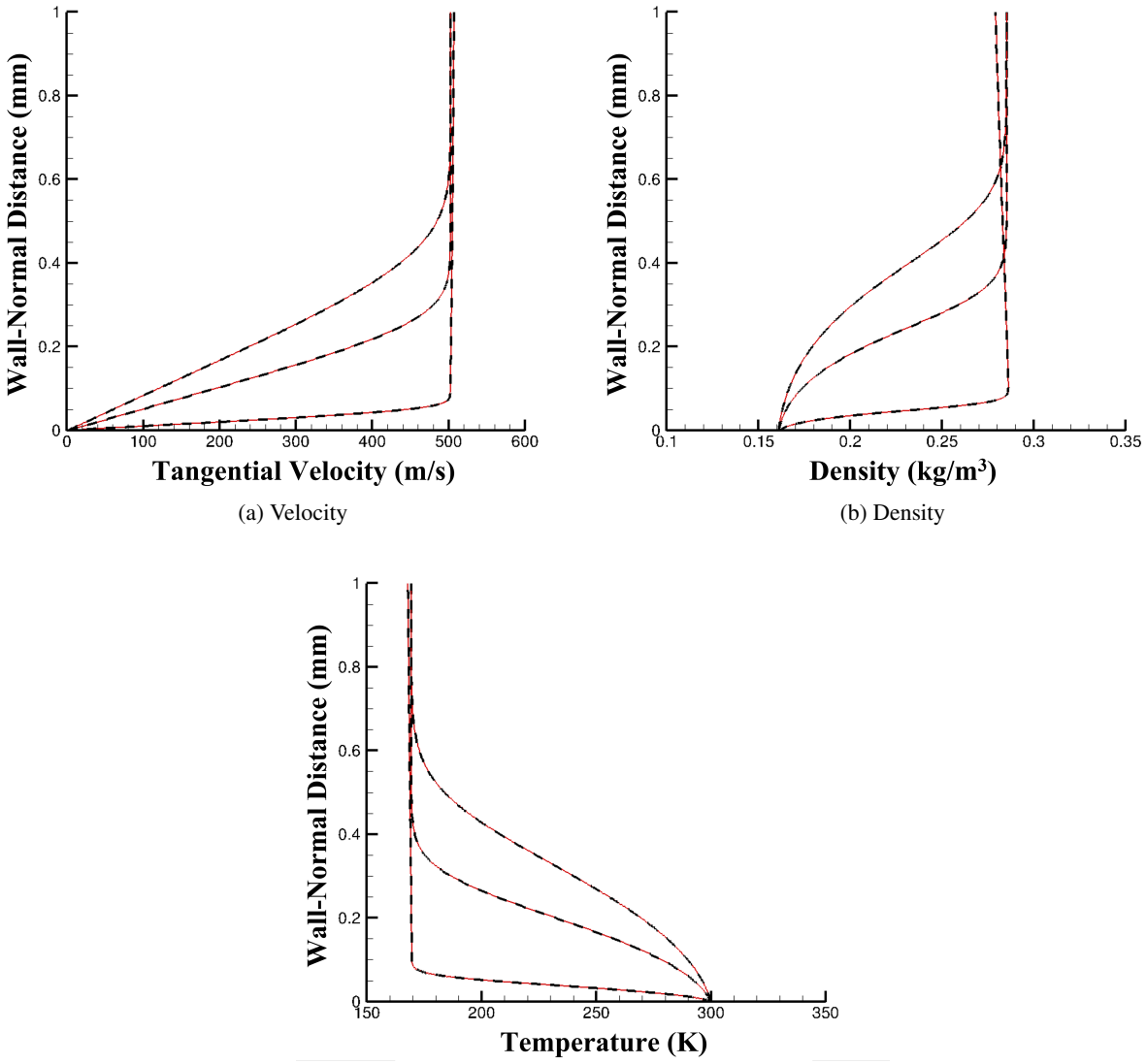


(a) Velocity

(b) Density

(c) Temperature

**Fig. 10 Comparison of mean flow profiles between OVEFLOW and VULCAN-CFD solutions at $\frac{x}{L}$ = 0.1, 0.5, and 0.8 axisymmetric flow of JAXA's straight cone model.**

Small differences between the present analysis and previously published results in the modes that are locally tangential to the N-factor curves were found along this streamline, and so a thorough analysis was conducted to isolate the source of the disagreement between the present and previously published N factor results. The possible causes identified were potential differences in the LASTRAC solver versions between the present analysis and the prior one, differences in the predictions caused by differences in the grid index-based marching used for structured grids and the fraction streamline length-based marching required for unstructured grids, and the influence of subsampling on the stability computation as discussed in section II.E.1. To evaluate the relative significance of these causes, N-factor curves from the previous analysis are compared to profiles generated using the base flow and inputs from that analysis but using the current version of the code. This is also compared to the Vulcan base flow analyzed using input parameters (except for the streamline path) generated by the automated routine. The VULCAN-CFD analysis was then compared to the equivalent structured OVERFLOW base flow, which in turn was compared to the unstructured base flow used by the automated routines. Figures 16 and 17 compare the N factors and growth rates for the interior streamline. As can be seen in these figures,

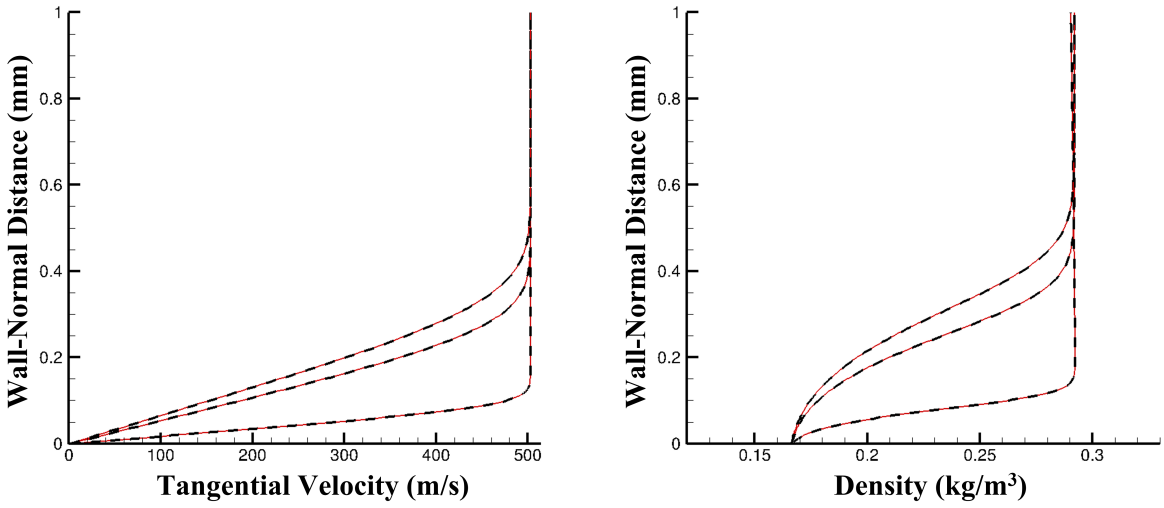


(a) Velocity

(b) Density

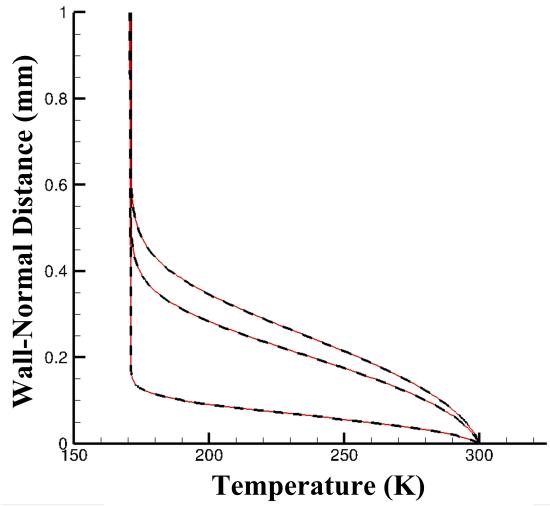


(c) Temperature

**Fig. 11 Comparison of mean flow profiles along the windward plane between OVEFLOW and VULCAN-CFD at $\frac{x}{L}$ = 0.1, 0.5, and 0.8 for JAXA's straight cone at 2° angle of attack.**

the overall disagreement between the individual N factor curves is approximately 0.3 at most, and this disagreement occurs downstream of the experimentally determined transition N-factor, which is approximately 7 along this streamline. From these figures, the main instance where this disagreement is introduced is in the comparison between the structured OVERFLOW base flow and the unstructured base flow. Analyzing the growth rates shows that the unstructured growth rates lag behind the structured analysis. Despite the small disagreement found in the three-dimensional crossflow streamline, the overall comparison was found to be satisfactory for the purposes of transition prediction, and further analysis is planned to isolate the cause of the disagreement.

## IV. Intermittency Parameters

This section presents the results of the analysis of the intermittency parameter calibration for the HIFiRE-1 [25] and LaRC Mach 3.5 Straight Cone [30] cases. Intermittency tuning was conducted with $k$ values initially ranging from 0.2 to 1.0, $C_1$ from 0.5 to 0.9, and $C_2$ from 1.05 to 1.2. Larger values of $C_2$ tend to extend the transition region downstream,

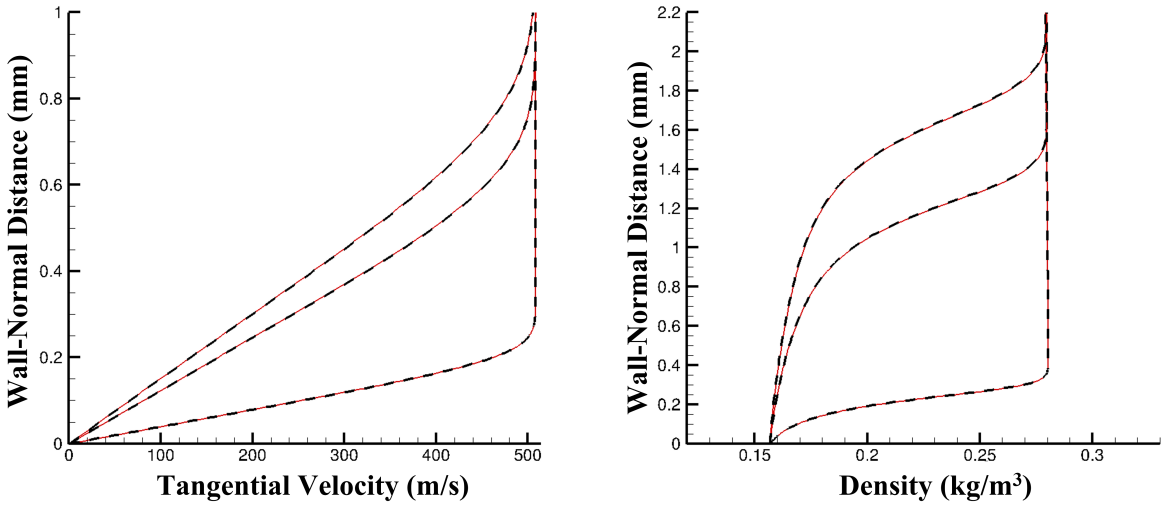


(b) Velocity

(b) Density

(c) Temperature

**Fig. 12 Comparison of mean flow profiles along the leeward plane between OVEFLOW and VULCAN-CFD at $\frac{x}{L}$ = 0.1, 0.5, and 0.8 for JAXA's straight cone at 2° angle of attack.**

which pushes it outside of the domain in some cases. Data visualization examines data in terms of $C_1$ and $\Delta C$ (defined as $C_2$ - $C_1$) rather than $C_1$ and $C_2$. For both cases, the first round of the tuning analysis examined 64 combinations of $k$, $C_1$, and $C_2$. As stated in section II.F, this analysis is conducted without consideration for improving the prediction of $N_{tr}$, and because the local slope of the N-factor curve is dependent on local N for a given test case this process does not produce a true optimization. However, investigation of $N_{tr}$ should begin by investigating the free-stream disturbance environment rather than the brute force approach taken here, but the investigation of $k$, $C_1$, and $C_2$ independent of $N_{tr}$ still provides insight into the characteristics of the coupled analysis method for high-speed flows.

Subsequent rounds of the analysis successively refined the envelope of the independent variables based on the best-performing parameters from the previous round. This analysis protocol was chosen to identify a single, best-performing set of parameters for each type of instability. Through the course of this analysis, it became apparent that, rather than a single point of minimum error, a subset of the independent variable space constitutes a region of best performance. When this was determined, the method of successive refinement was changed to manually identifying regions of coarse

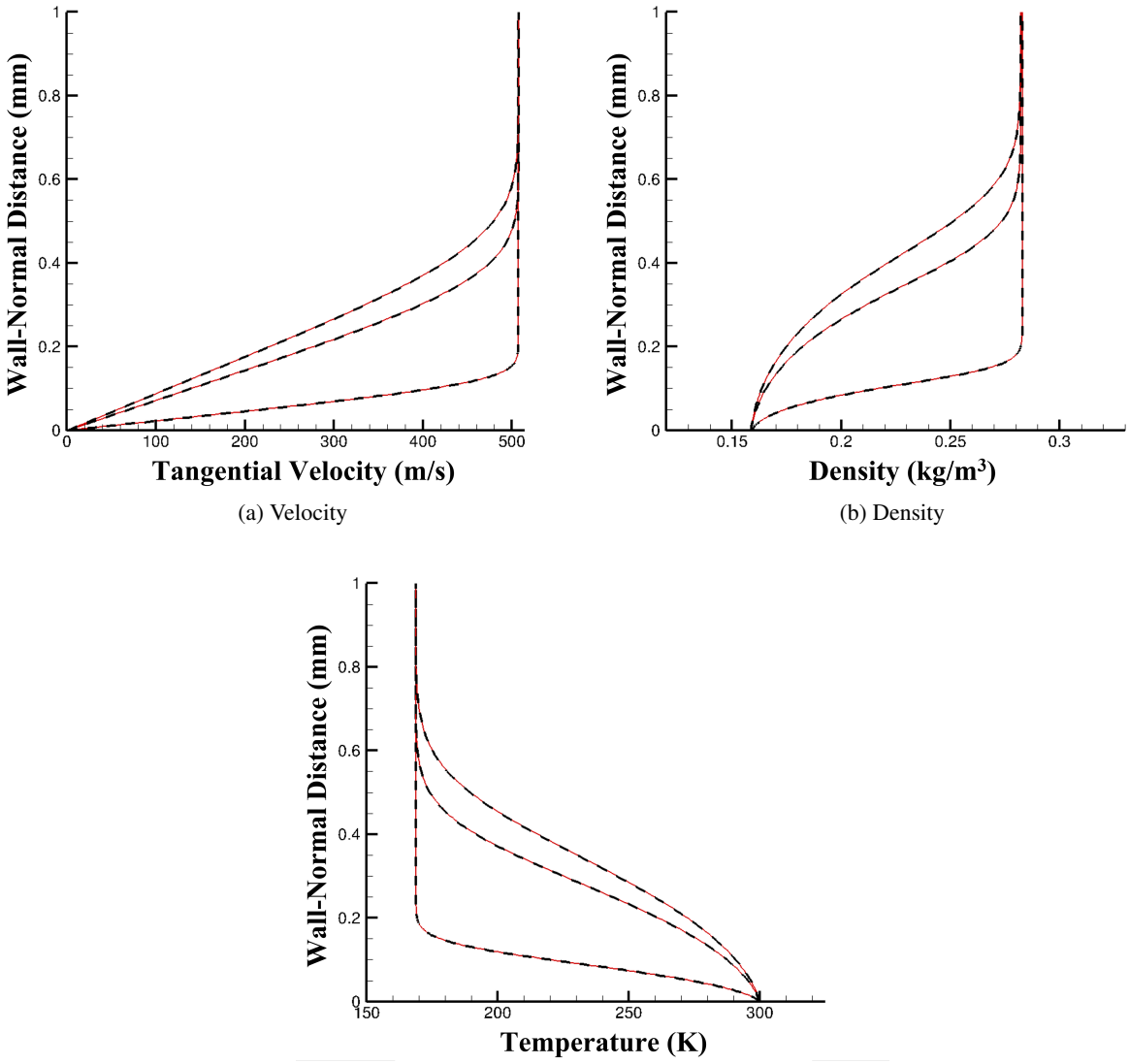


(a) Velocity

(b) Density

(c) Temperature

**Fig. 13 Comparison of mean flow profiles along the intermediate plane between OVEFLOW and VULCAN-CFD at $\frac{x}{L}$ = 0.1, 0.5, and 0.8 for JAXA's straight cone at 2° angle of attack.**

refinement in the independent variable space and examining them. The results of this analysis for both sets of tuning test cases are shown in Figs. 18 and 19.

The $2^{nd}$ mode analysis shows a wide region of the independent space where the error is near its minimum value. Therefore, any combination of parameters within this subset of the independent variable combinations examined is considered acceptable. Generally speaking, the wide band appears to be the result of conflicting trends in the intermittency width's response to changes in the independent variables. Specifically, increasing $k$ and decreasing $\Delta C$ have the effect of narrowing the transition region width, and decreasing $k$ and increasing $\Delta C$ have the opposite effect. It can be seen in Fig. 18 that cases with $k$ = 0.45 and $\Delta C$ = 0.3 have similar levels of error to cases with $k$ = 0.65 and $\Delta C$ = 0.5. Work is ongoing to run additional cases to identify the bounds of this variable space and identify a relationship between the independent variables that could be used to describe it.

Importantly, the parameter set based on the low speed applications of this method [21] of $k$ = 0.412, $C_1$ = 0.8 and $\Delta C$ = 0.3, lies at the edge of the band of best-performing inputs, and so changing the intermittency parameters will

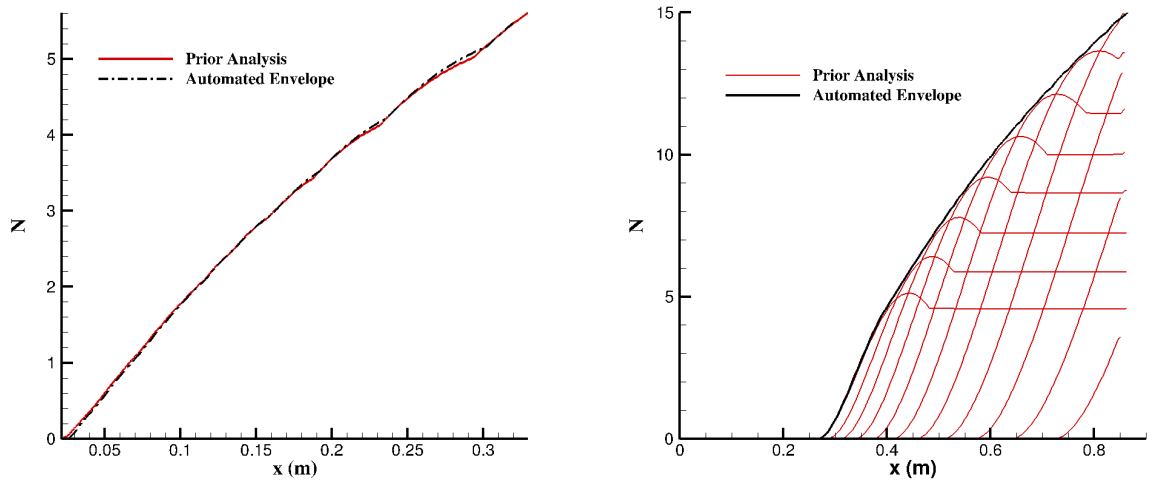


(a) JAXA SC1 axisymmetric case.

(b) HIFiRE -1 case at t = 21.5 s.

**Fig. 14 Comparision of the N factor envelope generated from the automated routine with that calculated by previous works [26, 29]. Results from the previous analysis for the HIFiRE case correspond to frequencies between 450 kHz and 725 kHz with increments of 25 kHz.**

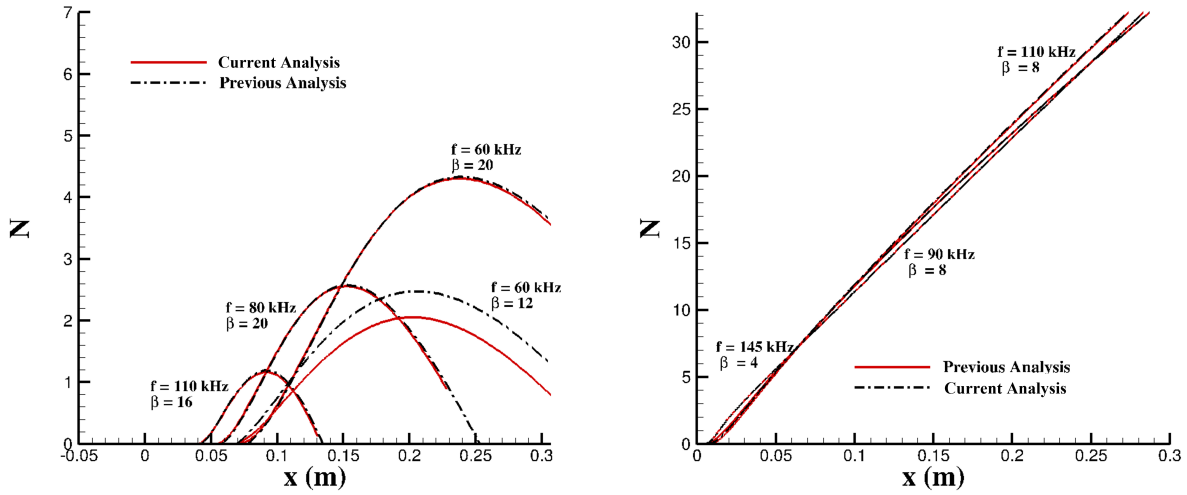


(a) Windward ray

(b) Leeward ray

**Fig. 15 Comparison of the current and previously published [29] LASTRAC analysis for the JAXA SC1 at 2° angle-of attack at the windward and leeward planes. Current analysis uses an unstructured-format base flow file which is generated from a subsampling of the OVERFLOW mean flow solution.**

likely not yield significant improvement in the transition width prediction for engineering purposes. This can be seen by directly comparing the transition results from the initial parameters to a point within the high-performing band. These results are presented in Figs. 20 and 21 respectively, and while the two sets of parameters do shift the location of transition onset, the feature of interest, namely, the transition zone width, is minimally impacted. In both Fig. 20 and 21, the analysis uses a constant $N_{tr}$ = 14.7, which is representative of the $N_{tr}$ for the suite of test cases. Because the data shown in Fig. 21 uses a lower value of $C_1$ (0.65 vs 0.8), the transition region is shifted upstream, but this is not a result of changes to $N_{tr}$ and predicting the precise transition location is, by design, not a goal of this exercise.

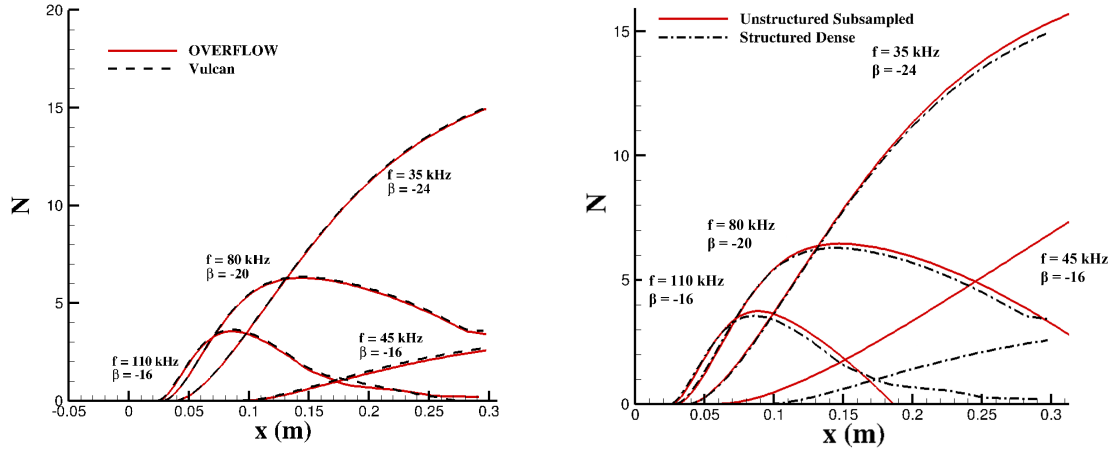


(a) Vulcan vs structured OVERFLOW

(b) structured OVERFLOW vs current

**Fig. 16 Comparison of the automated LASTRAC analysis using an unstructured base flow calculated from a sub-sampling of the original OVERFLOW mean flow, and a manually performed LASTRAC analysis using a structured mean flow file without subsampling for the JAXA SC1 at 2° angle-of attack at the intermediate streamline.**

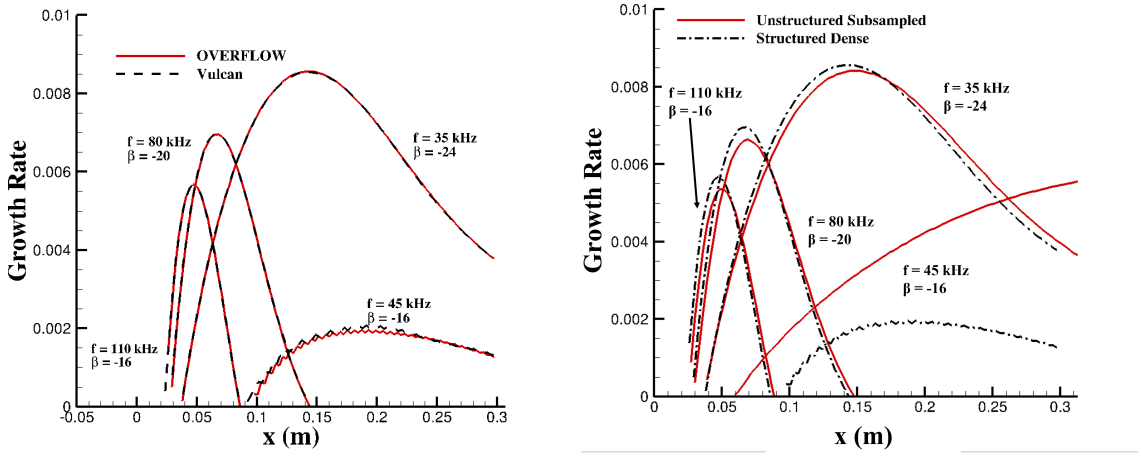


(a) Vulcan vs structured OVERFLOW

(b) structured OVERFLOW vs current

**Fig. 17 Comparison of growth rates from the automated LASTRAC analysis using an unstructured base flow calculated from a sub-sampling of the original OVERFLOW mean flow, and a manually performed LASTRAC analysis using a structured mean flow file without subsampling for the JAXA SC1 at 2° angle-of attack at the intermediate streamline.**

For the $1^{st}$ mode case the results are more straightforward. The analysis identifies a relatively narrow region of low error that falls nearly on top of the baseline parameters. The best performance was found using values of $k = 0.44$, $C_1 = 0.79$, and $\Delta C = 0.31$. These values are very similar to the baseline parameters of $k = 0.412$, $C_1 = 0.8$, and $\Delta C = 0.3$ and produce similar results. Keeping in mind that changing the intermittency parameters based on instability type would increase the complexity of the coupled analysis routines, it is deemed not worth the marginal change in results to change the parameters for $1^{st}$ mode transition.

Because neither parameter analysis warranted changes in the intermittency parameters used, all subsequent analysis presented uses the baseline parameters of $k = 0.412$, $C_1 = 0.8$, and $\Delta C = 0.3$. While it is found that these parameters are

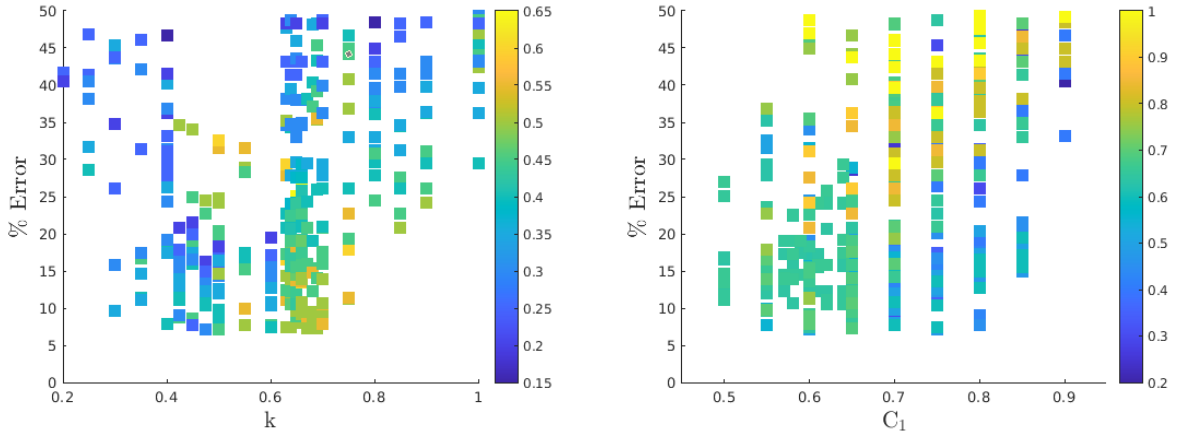


(a) Error vs. $k$ colored with $\Delta C$

(b) Error vs. $C_1$ colored with $k$

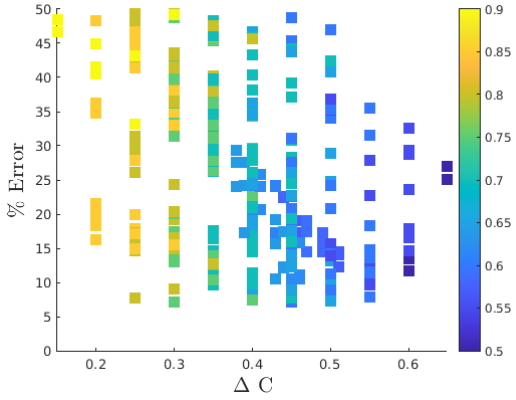


(c) Error vs. $\Delta C$ colored with $C_1$

**Fig. 18 Transition width error for the intermittency parameters examined for the $2^{nd}$-mode analysis. Analysis examines the HIFiRE-1 ascent phase transition profiles [25] at t = 19, 20, and 21 s.**

acceptable for the HIFiRE-1 and LARC Supersonic cone test cases, it remains to be seen whether this is the case in general or if this finding is specific to these test cases. The cases used to calibrate the intermittency are shown in Fig. 22

## V. Application to Additional Test Cases

This section examines the remainder of the test cases presented in this work. First, the axisymmetric test cases explored in this work for $2^{nd}$-mode and $1^{st}$-mode transition are examined. Next, the three-dimensional case examined here using the coupled methodology is presented and discussed, and finally a discussion of the next steps required in the development of the coupled analysis is presented including some exploration of influence of mesh quality on the results.

### A. Mack's $2^{nd}$-Mode Test Cases

The first axisymmetric test case examined is the t = 22 s case from the HIFiRE-1 flow condition set. This case was omitted from intermittency tuning because the experimental data show the transition region leaving the domain, and so the width could not be easily evaluated. The results of this case, shown in Fig. 23, demonstrate that transition profiles that intersect with the domain exit plane can be captured by the coupled analysis. This is of interest because this interferes with the calculation of $x_{tr}$ in the prescription of the intermittency profile, and this case tests the method's ability to extrapolate $x_{tr}$ beyond the domain.

The next test case examined is that corresponding to the experiments performed by Horvath et al. [28]. This case is

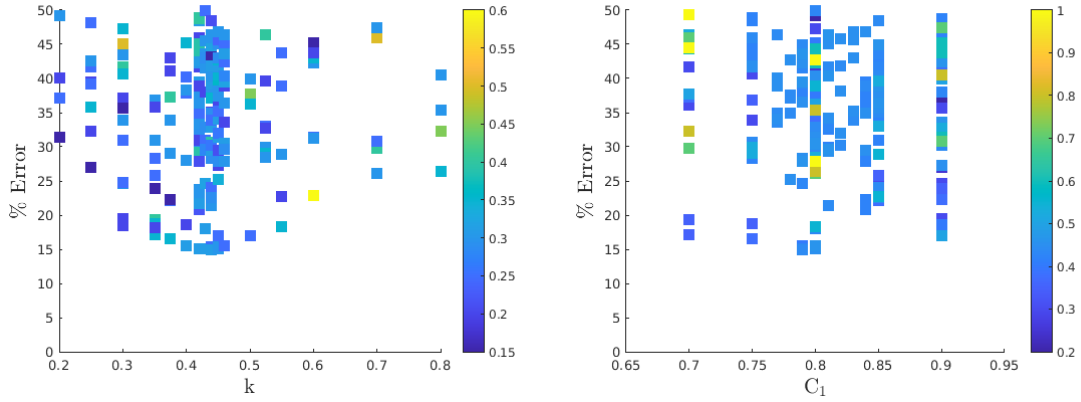


(a) Error vs. $k$ colored with $\Delta C$

(b) Error vs. $C_1$ colored with $k$

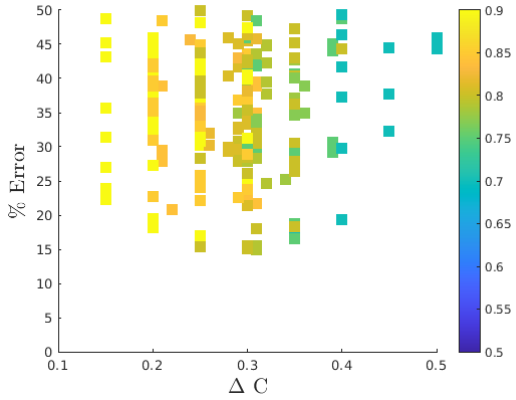


(c) Error vs. $\Delta C$ colored with $C_1$

**Fig. 19 Transition width error for the intermittency parameters examined for the $1^{st}$-mode analysis. Analysis compares computed data to that of Chen et al. [30] for cases with Re = 7.80, 5.89, and 3.85 $\times$ $10^7$ $m^{-1}$**

one sample from the set of the straight cone runs in the NASA 20-inch Mach 6 wind tunnel. The results of the coupled compuatation are shown in Fig. 24. For this case, the value of $N_{tr}$ was not provided in the literature, but the transition locations on the body for each test case are known. The value of $N_{tr}$ for this case was determined using laminar base flows calculated as a part of this study. The value of $N_{tr}$ for the case examined here is 5.5. A necessary future step in developing the coupled analysis capability is to identify a means of predicting $N_{tr}$ without these precursor analyses. Several key observations can be made from these results. Firstly, the transition onset location observed in the CFD results is significantly downstream of the point at which transition is predicted in the LST analysis. The LST analysis is found to agree closely with the experiments in identifying the point at which transition occurs. Indeed, it is apparent that transition onset does not begin until the value of $\gamma$ is nearly 0.8. This behavior was found to be mesh independent.

A key factor which differentiates these test cases from the HIFiRE suite of cases, which are the other set used to evaluate $2^{nd}$-mode induced transition, is the use of the SST turbulence model instead of SA. For this case, the SA model was found to predict poor results in the turbulent region, and this phenomenon is being investigated.

It is also observed that the transition region for this case is too narrow relative to the experiment in all cases. Interestingly, the end of the transition zone appears to be approximately correctly placed in all cases and combined with the accurate prediction of the transition location, this suggests that it is the delay in response to the prescribed intermittency that leads to this overly narrow transition zone. Again, this may be the result of the difference in turbulence model used between this case and the others, and research is ongoing to characterize the impact of turbulence model choice on the transition behavior given a specified $\gamma$ profile for which both SA and SST yield high-quality results. What can be clearly ascertained is that the baseline intermittency width parameters are not adequate for all hypersonic CFD cases, though the exact circumstances in which they should be altered and how they should be altered based on the other

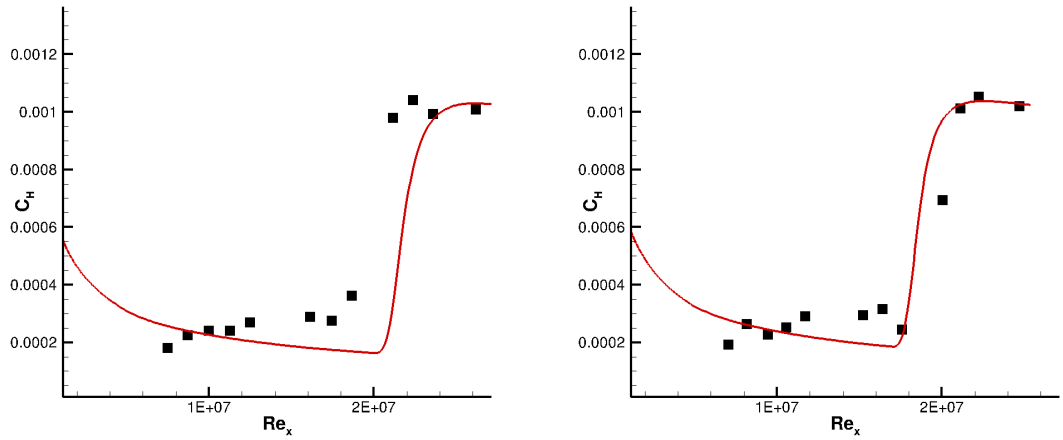


(a) $t$ = 19 s




(b) $t$ = 20 s

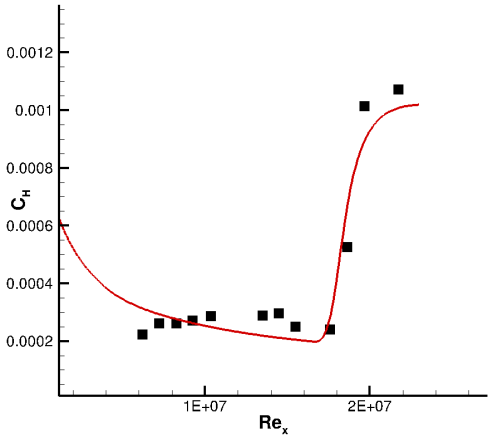


(c) $t$ = 21 s

**Fig. 20 Heat transfer prediction for the training subset of HiFIRE-1 cases using the baseline parameters of $k$ = 0.412, $C_1$ = 0.8, and $C_2$ = 1.1. $N_{tr}$ = 14.7 for these cases.**

.

flow, geometry, and simulation parameters requires further investigation.

### B. Mack's 1$^{st}$-Mode Test Cases

The final set of axisymmetric test cases examined is the LaRC Mach 3.5 supersonic cone. All five of the test cases in that suite examined in this work are shown in Fig. 25. As can be seen, the intermittency parameters perform reasonably well across the suite of test cases. The overshoot phenomena observed in some of the experimental cases is not captured, and changes to the imposed intermittency profile that allows for values of $\gamma$ exceeding 1.0 would be necessary to achieve this. Despite this, the automated routine reliably predicts transition widths that match the experimental data reasonably well. The Mach 3.5 cases used to tune the intermittency parameters used a constant representative value of $N_{tr}$ = 9. In order to visually compare the computational results with the experiment, it was necessary to tweak the value of $N_{tr}$ slightly on a case-by-case basis to overlay well with the experimental transition location. This may be a result of the "scalloping" phenomena observed in some automated N factor envelopes due to the discrete envelope of modes not fully describing the continuum of frequencies present on the real body. This can be alleviated by increasing the density of frequency/wave angle combinations examined. This increases the computation time but also the fidelity of the solution.

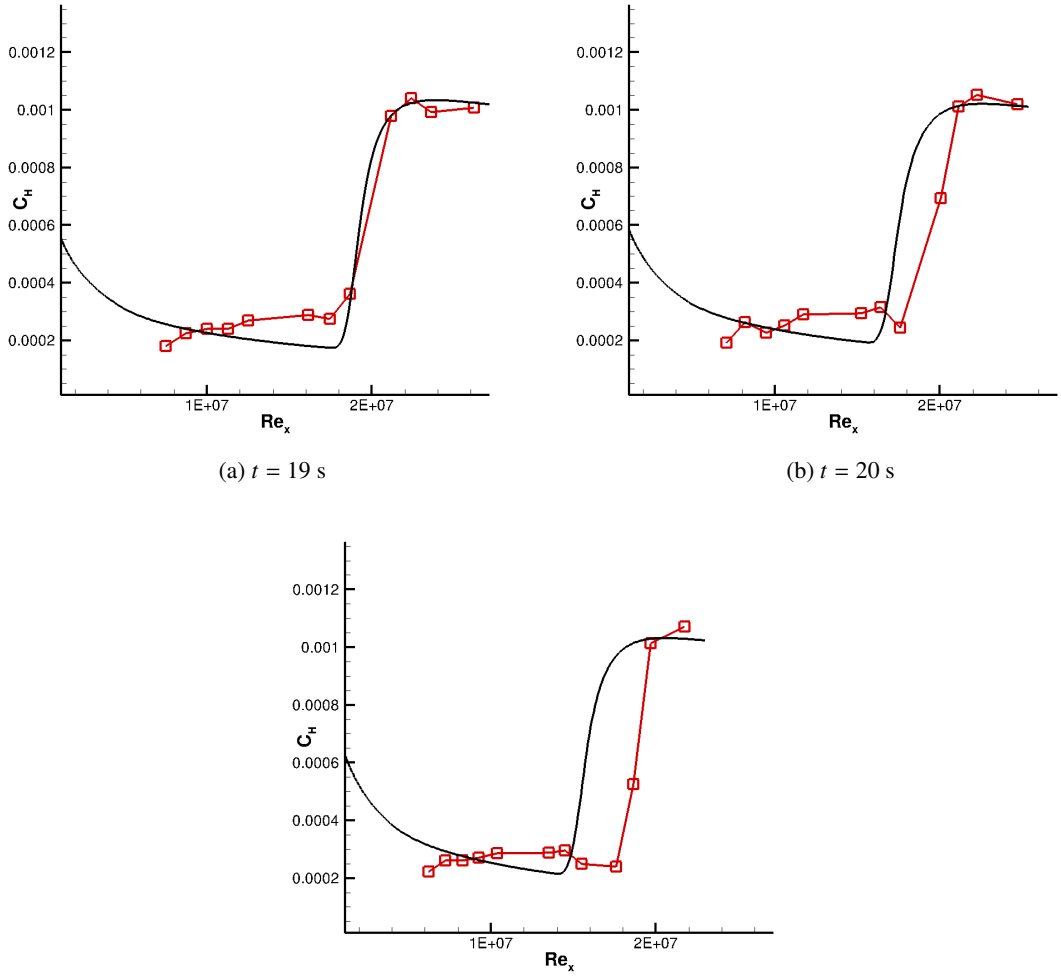


(a) $t$ = 19 s

(b) $t$ = 20 s

(c) $t$ = 21 s

**Fig. 21 Heat transfer prediction for the training subset of HiFIRE-1 cases using $k$ = 0.64, $C_1$ = 0.65, and $C_2$ = 1.05. $N_{tr}$ = 14.7 for these cases.**

### C. JAXA Three-Dimensional Test Case

The final test case examined in this work is the JAXA SC1 geometry at 2° angle-of-attack. This case represents a proof-of-concept for the application of the coupled OVERFLOW-LASTRAC analysis to 3D cases at supersonic Mach numbers. This case is also the first use of the fully automated analysis for a three-dimensional case, and the first time the distributed intermittency profiles used in this work have been applied to a 3D case within this coupled CFD-LASTRAC framework.

This case introduces several challenges not faced by the axisymmetric cases. The first challenge is file size; the current version of the plot3d-to-unstructured file conversion tool is limited in input file size, which precluded the analysis of the entire grid. Presently, files to be converted are limited to an input file size of 2 GB, and this limitation will be addressed in the future. To circumvent this limitation, OVERFLOW's domain subsampling functionality was used to create a plot3d-formatted subset of the domain for stability analysis. This subset trimmed the region near the nose from the domain, as it is densely packed with grid points and not relevant to stability analysis and subsampled the mesh in the streamwise direction to 50% mesh density. With the grid subsampling, the generation of the unstructured LASTRAC-format mean flow file for stability analysis takes approximately 5 hours on 16 processors. This is much greater than the time required for the axisymmetric cases, which for a typical case in this work was less than one minute. The impact of this subsampling has been partially explored in section III.C, and will be examined in isolation in the

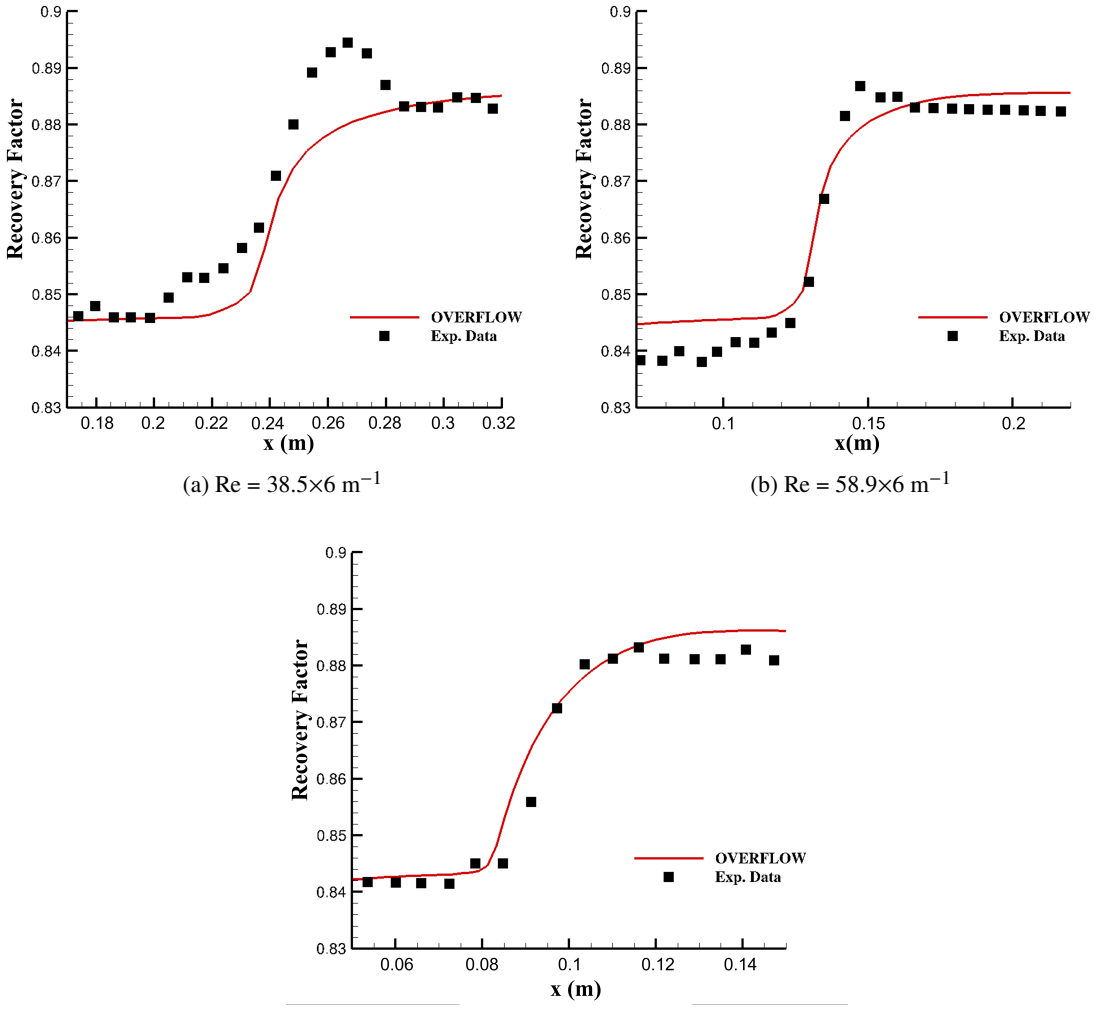


(a) Re = 38.5×6 m$^{-1}$

(b) Re = 58.9×6 m$^{-1}$

(c) Re = 78.0×6 m$^{-1}$

**Fig. 22 Comparison of coupled transition prediction results to the experimental data of Chen et al. [30] for the cases used to tune the intermittency parameters. For these cases a nominal value of $N_{tr}$ = 9.0 is used.**

following section for a different test case. Improvement of the conversion tools to avoid the need for subsampling is a priority in the further development of the coupled methodology.

The next aspect of the three-dimensional analysis that is not included in the axisymmetric cases is streamline seeding and streamline-aligned calculations. For this case, 32 streamlines were calculated from seed points near the upstream extent of the subsampled domain. LASTRAC stability analysis is conducted along each streamline to calculate the N factor profile along it. These analyses are run in parallel with one another. The automated routine for this case scanned both frequency and wave number, and so would capture both Mack's $1^{st}$ and crossflow modes. The overall computational wall time required for the analysis is similar to the $1^{st}$-mode computation, but the computational resources required are greater by a factor of the number of streamlines examined. With the N-factor profiles along the streamlines calculated, Eqn. 6 is applied to Gaussian intermittency distribution along the streamline. Figure 26 shows the N-factor and resultant intermittency function file after the initial stability analysis iteration is completed. Some jaggedness is observed in the intermittency profile, and while this has thus far not prevented the analysis from functioning, it is desirable to remove this jaggedness as it may hamper the convergence of the iterative method. For this case, $N_{tr}$ = 7 was chosen by comparing the stability results and experimental transition locations presented in Ref. [29].

The authors note that the choice of integration trajectories for a fully three-dimensional flow is rather ad hoc, in

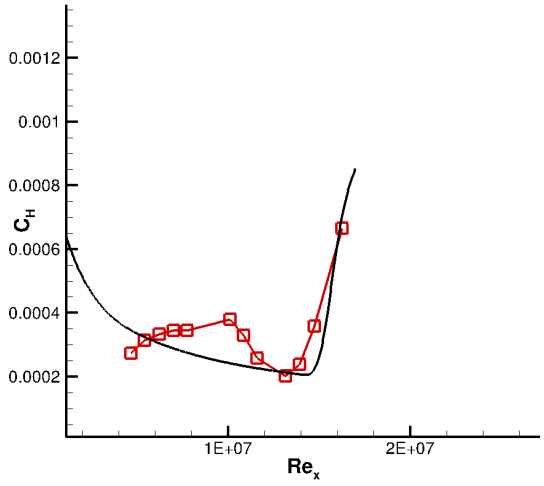


**Fig. 23 Stanton number distribution predicted for the HIFiRE-1 cone at conditions corresponding to $t$ = 22 s in the experiment. $N_{tr}$ = 14.7 for this case.**

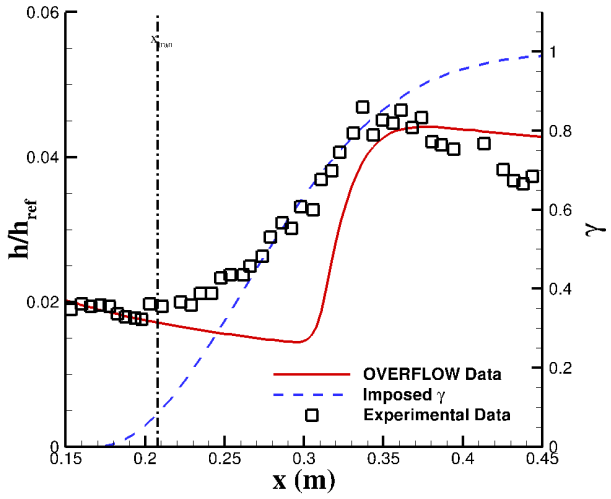


**Fig. 24 Comparison of coupled transition prediction results to the straight cone data of Horvath et al. [28] with Re = 14.1×6 m$^{-1}$, $R_n$ = 0.00254 mm, and $M_\infty$ = 6. Values of $x_{tran}$ are predicted by LST and imposed via the coupled methodology. $N_{tr}$ = 5.5 for this cases.**

general. The purpose of this exercise is to evaluate the ability of the coupled solver to work with a specified set of trajectories, which is chosen to be streamlines. However, similar analysis could be conducted based on other options such as vortex tracks with axially varying azimuthal wavelength, etc.

Fig. 27 shows the skin friction distribution on the JAXA SC1 cone after 3 iterations of the coupled analysis. This figure also displays skin friction in $\Phi$-$Re_x$ space for comparison to the experiment. As can be seen, the coupled analysis performs well in the mid portion of the cone away from the leeward plane but does not capture the advancement of the transition front as one approaches the leeward ray. Instead, the stability analysis predicts the transition front retreating downstream as the azimuthal position approaches 0°. This is, however, consistent with the stability calculations in Ref. [29], which found that the isolines of N factor peak in the mid-part of the cone and retreat downstream as they move toward the azimuth. As discussed in section III.C, capturing the spike in N factor at the leeward plane required careful

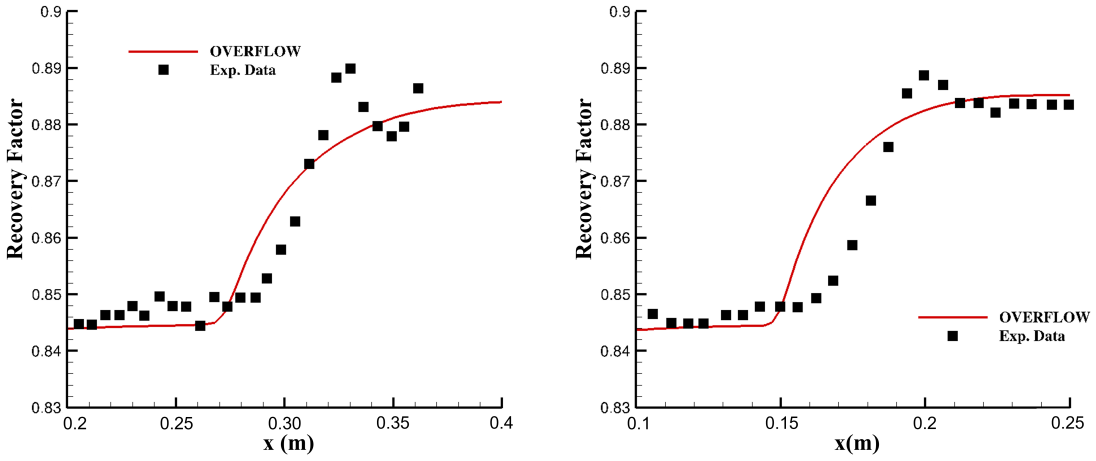


(a) Re = 28.1×6 m$^{-1}$ (b) Re = 49.0×6 m$^{-1}$

**Fig. 25 Comparison of coupled transition prediction results to the experimental data of Chen et al. [30] for the cases not used to tune the intermittency parameters. For these cases, a nominal value of $N_{tr}$ = 9.0 is used.**

selection of streamline seed point, and the analysis presented in Fig. 27 did not yet incorporate that learned lesson.

It should also be noted that LST is insufficient to capture the transition behavior in this region. In the mean flow, a narrow bulge appears near the leeward ray that is the result of rollup from the secondary flow from both sides of the cone converging. The rapid azimuthal variations associated with this narrow structure necessitates a multidimensional stability analysis [36]. This type of analysis requires significantly more computational resources than the conventional N-factor integration along individual trajectories. Furthermore, the streak near the leeward ray can support multiple instability modes, making it difficult for regular CFD users to perform such analysis. Integration of streak instabilities into the automated process will be address in the future. To fully capture the transition behavior in this case, a multi-modal analysis that considers other types of instabilities in addition to traveling crossflow must be implemented.

Overall, the JAXA SC1 case at angle-of-attack represents a promising proof-of-concept for the three-dimensional automated and coupled analysis. The test case demonstrates that the coupled methodology can produce good results for 3D cases, but also demonstrates what gaps must still be filled before this methodology can be reliably applied to general 3D cases.

### D. Investigation of M = 6 Cone Transition

The results of the investigation of the LaRC Mach 6 straight cone require some elaboration. For this case, additional investigation is undertaken to evaluate whether the distributed intermittency model used in the coupled process provides significant advantages over a simple trip line specification for the transition location. To accomplish this, an intermittency file was generated with a step function distribution and the resulting heat flux distribution is compared to that predicted by the coupled solver analysis with a Gaussian intermittency distribution. The results of this analysis are shown in Fig. 28. The apparent transition zone is found to be approximately equal in width for both cases. It is also observed that the upstream extent of the transition region is still downstream of the imposed rise in intermittency even for the trip line case. This is also being investigated at the time of writing.

This suite of test cases also showed that the observed influence of transition, a sharp increase in surface heat flux, did not occur until the value of intermittency was relatively large. For the LaRC M = 6 cone database the observed upstream extent of the transition region corresponded to a value greater than 0.6 for all cases. If other cases exhibit similar behavior, it would be necessary to reconsider the current method of prescribing intermittency because the current method usually produces intermittency values of less than 0.5 at the predicted $x_{tr}$ location. To examine this, a representative sample case from each of the suites examined here is presented in Fig. 29. As can be seen in this figure, for the LaRC M = 3.5 cone, the HIFiRE-1 cone, and the JAXA M = 2 cone, the point at which the quantity of interest begins the sharp rise associated with transition at a location corresponding to an intermittency value of 0.5 or less.

In Fig. 29, the JAXA cone results show the surface quantities along a streamwise grid line that passes through the

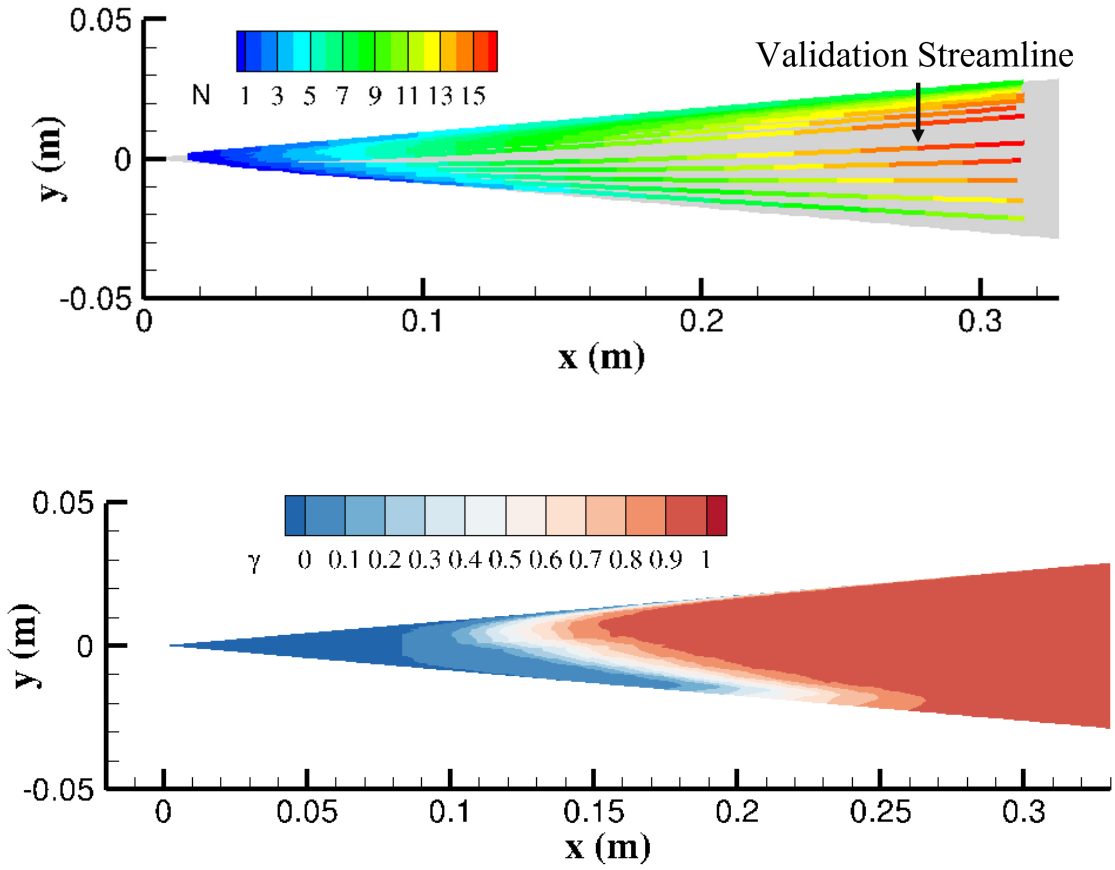


**Fig. 26 Visualization of the intermittency prescription process for the JAXA 3d cone. For this case, $N_{tr}$ = 7.0.**

region where the transition front reaches farthest upstream. The results of the overall set of cases examined in this work show that the relatively delayed transition behavior found in the LaRC M = 6 cone cases is different from the trends observed in the other test cases examined. Therefore, further investigation into the computations corresponding to the cases presented in Ref. [28] is ongoing, beginning with the possibility that the difference in turbulence model between these cases and the others studied here is the cause of this phenomenon.

### E. Preliminary Investigation of Grid Quality Dependence

As the OVERFLOW-LASTRAC coupled analysis frameworks continues to mature, it is necessary to examine aspects of the practical CFD analysis. The goal of creating the coupled methodology is to remove the expertise barrier normally in place for stability-based transition prediction. One aspect of this stability expertise is the knowledge necessary to create the very high-quality meshes that are generally considered necessary for stability analysis. Therefore, it is necessary to evaluate the ability of the automated stability analysis to calculate N factor profiles for cases where the underlying mesh does not meet the general guidelines for stability analysis.

To begin the process of evaluating the methodology for suboptimal grids, three additional permutations of the HIFiRE-1 test case at t = 20 s were created. The first of these is a conventional computational mesh with a constant wall-normal spacing and growth rate. In the region just downstream of the nose this mesh has approximately 150 points in the boundary layer and wall-normal growth rates at all streamwise stations are below 1.05. This grid was

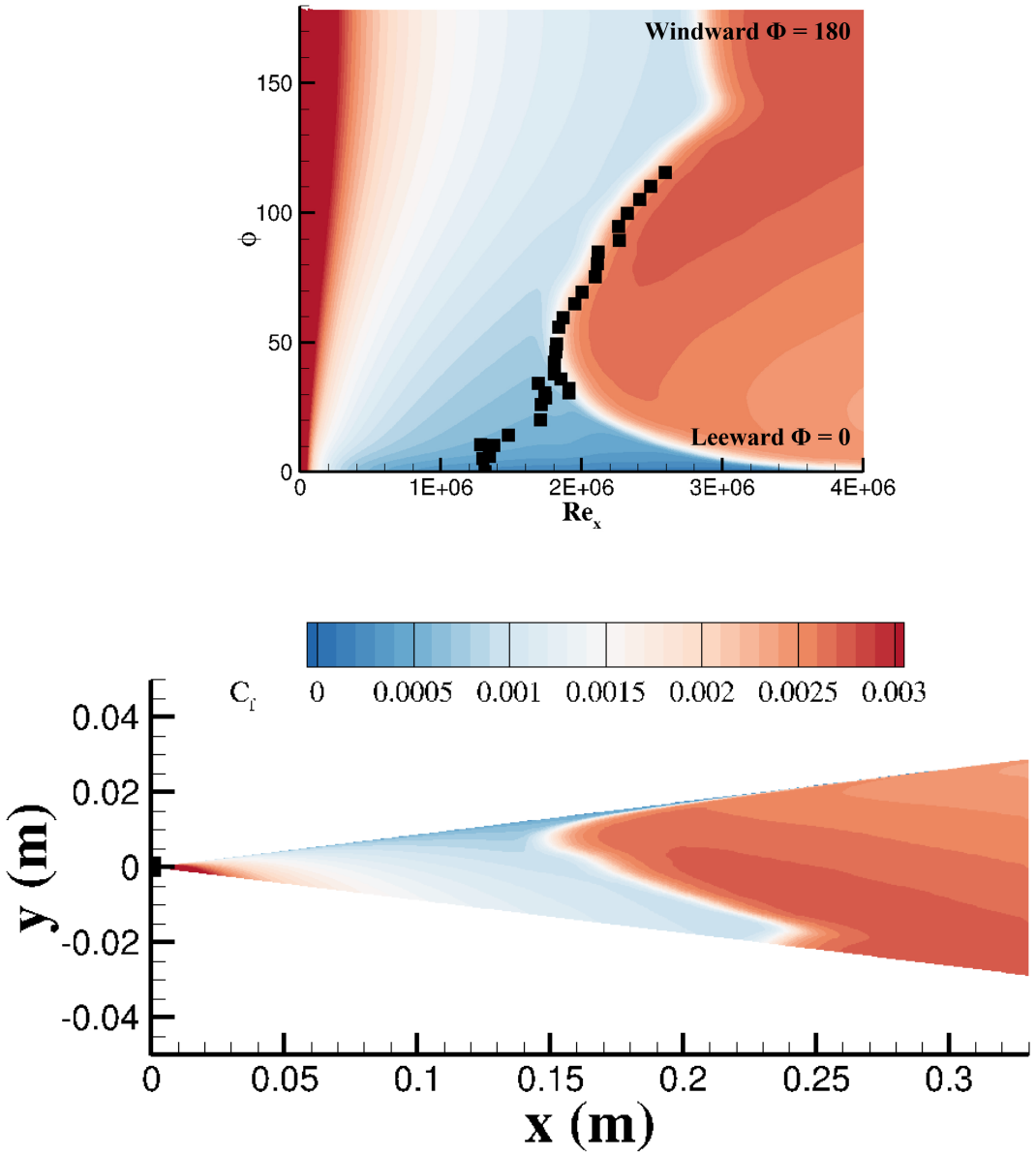


**Fig. 27 Skin friction coefficient predicted after 3 iterations of CFD-LASTRAC analysis.**

made such that $y^+$ immediately downstream of the nose was approximately 0.1. The next case is a subsampling of the shock-aligned, stability-quality mesh that is generated by extracting every other point in the streamwise direction. This case does not entail that a new CFD calculation is carried out but is generated from the existing stability-quality solution. The final case is generated by using the subsampled mesh from the previous case as the initial mesh for the CFD calculation and then calculating stability results from that. Unlike the previous case, this does involve the execution of a new OVERFLOW computation.

Figure 30 shows the N-factor envelopes calculated from each of these, along with the N-factor envelope calculated using the original base flow solution. This figure shows that of the three cases only the one calculated on the subsampled mesh produces rather different stability results. This case appears to miss some high-frequency modes which are amplified near the nose of the cone, but accurately captures the lower-frequency modes that lead to transition farther downstream. The precise cause of the omitted modes is still not fully characterized, but it should be noted that the uniform streamwise subsampling is likely most detrimental to the quality of the base flow in the region near the nose where the omitted modes should be. In the original grid, tight streamwise clustering was employed to ensure the nose

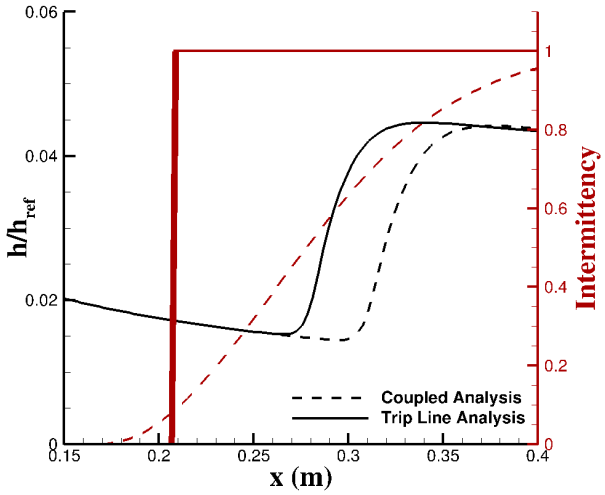


**Fig. 28 Comparison of the coupled analysis to a trip line specification for the LaRC M = 6 straight cone at $Re$ = 14.1 $\times$ $10^6$ $m^{-1}$. $N_{tr}$ = 7.2 for this case.**

curvature and bow shock are adequately defined. It is therefore not surprising that the first signs of decline in solution quality appear in this region. Overall, this is a promising result, as it indicates that the N-factor curves at sufficiently high N-factors are not sensitive to solution subsampling for this case, which supports the use of solution subsampling in the 3D analysis. This also indicates that conventional meshes with sufficient resolution can provide high-quality predictions using this method.

In the future, further analysis of this type will need to be conducted to examine cases with lower-order numerical schemes, base flows which are not fully grid-converged, and conventional grids with decreased resolution. Still, this result is a promising indicator that coupled stability-CFD analysis can be developed such that it could perform reliably in industrial context, even in the hands of a CFD user without significant experience in stability theory.

### F. Discussion of Next Steps

Overall, this work represents a progress report on the ongoing efforts to develop robust OVERFLOW-LASTRAC coupled transition prediction capabilities. This work specifically documents the extension of this capability to high-speed flows and demonstrates this capability across a variety of test cases. The results of this effort are promising, but many areas still require further exploration and development. A thorough investigation of the influence of turbulence model and numerical parameters is warranted considering the potential influence of those parameters on the CFD solver's response to applied intermittency profiles in the $2^{nd}$-mode cases. Further development will be necessary to expand the $1^{st}$-mode analysis beyond axisymmetric cases, and both this case and the traveling crossflow analysis tool will require further tuning to ensure robust predictions across multiple test cases. A relationship for $N_{tr}$ must be identified so that the analysis is not dependent on precursor stability analysis or existing data.

Improvements to the utilities which enable the coupled analysis are planned to make the 3D analysis less dependent on grid subsampling, and utilities which allow for automated mixed-mode transition predictions should be developed. Additionally, the coupled methodology must be tested on more challenging mean flows common in high-speed applications such as shock wave-boundary layer interactions. Finally, the supersonic coupled analysis should be evaluated for PSE stability computations to increase the accuracy of the stability predictions, especially for $1^{st}$-mode analysis.

Additional test cases are also planned to further evaluate the capabilities of the present method. Most notably, a second three-dimensional test case is planned to examine the HIFiRE-5 elliptical cone geometry. This case will be used to evaluate means of integrating the stability analyses for crossflow instabilities and Mack's $2^{nd}$ mode together on a single flight configuration.

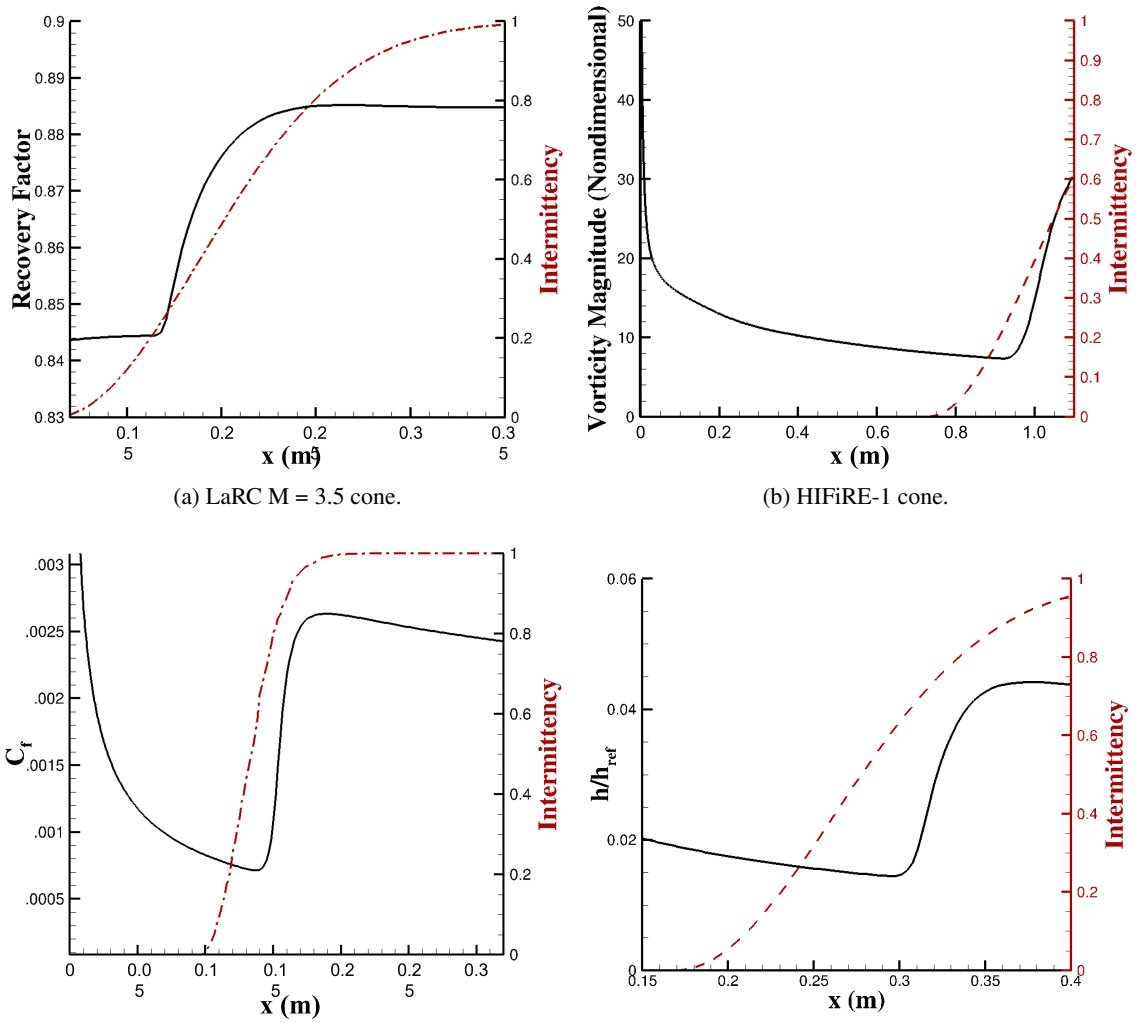


(a) LaRC M = 3.5 cone.

(b) HIFiRE-1 cone.

(c) JAXA M = 2 cone.

(d) LaRC M = 6 cone.

**Fig. 29 Comparision of intermittency distribution with quantity of interest for selected cases. Conditions correspond to (a) the LaRC 5dSCS with $M_\infty$ = 3.5, $N_{tr}$ = 9, and $Re$ = 49.0 $\times$ $10^6$ $m^{-1}$, (b) the HIFiRE-1 cone at t = 22 s with $M_\infty$ = 5.31, $N_{tr}$ = 14.7, and $Re$ = 11.74 $\times$ $10^6$ $m^{-1}$, (c) the JAXA straight cone at 2° angle of attack with $M_\infty$ = 2.0, $N_{tr}$ = 7, and $Re$ = 12.2 $\times$ $10^6$ $m^{-1}$, and (d) the LaRC 5dSCH with $M_\infty$ = 6.0, $N_{tr}$ = 7.2, and $Re$ = 14.1 $\times$ $10^6$ $m^{-1}$.**

## VI. Summary and Conclusions

A methodology for predicting laminar-turbulent transition for high-speed flows using OVERFLOW 2.3 coupled to the LASTRAC stability analysis software has been described and demonstrated for transition caused by Mack's $1^{st}$ and $2^{nd}$ mode instabilities as well as crossflow modes. This work provides details of one specific part of a wider and ongoing effort to make transition prediction via stability analysis possible for CFD practitioners without stability expertise via coupled and automated analysis. This work analyzed multiple test cases across the high-speed regime and evaluated the intermittency modeling parameters used in the automated analysis. While the parameters used for low-speed flows were found to be adequate for most cases analyzed, some cases were identified for which the existing parameters were not adequate. Investigation is ongoing to examine other variables, such as turbulence model choice, in interpreting these results. The automated coupled analysis was demonstrated for a supersonic boundary layer over a cone at 2° angle of attack, and the transition front predicted was found to be in good agreement with the available experimental data within the limits of the LST analysis. Finally, a cursory analysis of the influence of reduced

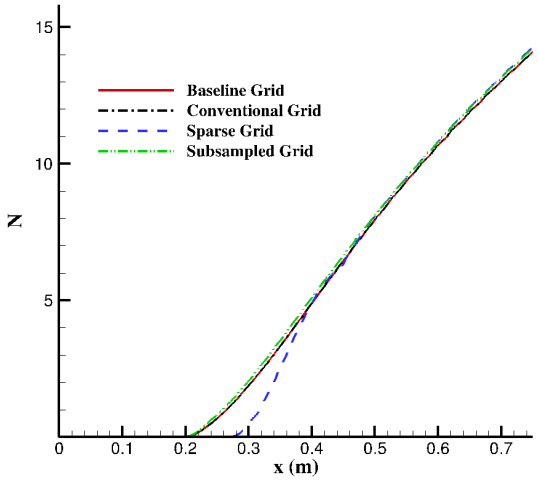


**Fig. 30 N-factor envelope for the HIFiRE case with reduced-quality meshes.**

mesh quality on the automated stability analysis is conducted, which suggests that reasonable results can be obtained for conventional grids with adequate resolution. The coupled prediction of transition for high-speed flows has been demonstrated for a representative set of canonical high-speed flow configurations. In the course of this demonstration, areas that require further development to increase the robustness and reliability of the method have been identified. Despite these remaining challenges, this work represents a critical step in the development of a general-purpose coupled transition prediction framework, and efforts are ongoing to mature the capability further by addressing the remaining technical objectives.

## Acknowledgments

This research is sponsored by the NASA Hypersonic Technology Project and the NASA Transformative Technology Project (TTT) under the Aeronautics Research Mission Directorate. The research of the NIA authors is funded by the NASA Langley Research Center through the cooperative agreement 2A00 with the National Institute of Aerospace (NIA). The computing resources used in this work were provided by the NASA Langley Research Center's K-Midrange Cluster and by the NASA High-End Computing (HEC) Program.

## References

[1] Slotnick, J., Khodadoust, A., Alonso, J., Darmofal, D., Gropp, W., Lurie, E., and Mavriplis, D., "CFD Vision 2030 Study: A Path to Revolutionary Computational Aerosciences," 2014. NASA/CR-2014-218178.

[2] Anderson Jr, J. D., *Hypersonic and High-Temperature Gas Dynamics*, American Institute of Aeronautics and Astronautics, 2019. https://doi.org/10.2514/4.105142, 3rd Edition.

[3] Mack, L., "Boundary Layer Linear Stability Theory (Special Course on Stability and Transition of Laminar Flow)," , 1984. AGARD-R-709, Neuilly-Sur-Siene, France.

[4] Hader, C., and Fasel, H. F., "Towards Simulating Natural Transition in Hypersonic Boundary Layers via Random Inflow Disturbances," *Journal of Fluid Mechanics*, Vol. 870, 2018, pp. R3–1 – R3–14. https://doi.org/10.1017/jfm.2018.386.

[5] Tufts, M. W., Borg, M. P., Bisek, N. J., and Kimmel, R. L., "High-Fidelity Simulation of HIFiRE-5 Boundary-Layer Transition," *AIAA Journal*, Vol. 60, No. 4, 2022, pp. 2039 – 2050. https://doi.org/10.2414/1.J060090.

[6] Goodwin, G. B., Bachman, C. L., Johnson, R. F., and Kessler, D. A., "Synethetic Freestream Turbulence Generation at an Inflow Boundary Condition," *AIAA SciTech Forum 2021*, American Institute of Aeronautics and Astronautics, 2021. https://doi.org/10.2514/6.2021-1846.

[7] Menter, F. R., Langtry, R., and Völker, S., "Transition Modelling for General Purpose CFD Codes," *Flow Turbulence and Combustion*, Vol. 77, 2006, pp. 277 – 303. https://doi.org/10.1007/s10494-9047-1.

[8] Menter, F., Smirnov, P. E., Liu, T., and Avancha, R., "A One-Equation Local Correlation-Based Transition Model," *Flow, Turbulence and Combustion*, Vol. 95, 2015, pp. 583–619.

[9] Coder, J. G., Pulliam, T. H., and Jensen, J. C., "Contributions to HiLiftPW-3 Using Structured, Overset Grid Methods," *AIAA Scitech Forum 2018*, 2018. https://doi.org/10.2514/6.2018-1039.

[10] Groot, K. J., Patel, J. M., Saiyasak, C. A., Coder, J. G., Stefanski, D. L., and Reed, H. L., "Assessment of the Amplification Factor Transport Transition Model for High-Mach Number Flows," *AIAA Aviation Forum 2021*, American Institute of Aeronautics and Astronautics, 2021. https://doi.org/10.2514/6.2021-2830.

[11] Paredes, P., Venkatachari, B., Derlaga, J. M., Choudhari, P. G. B. M. M., Li, F., and Chang, C.-L., "Assessment of RANS-based Transition Models based on Experimental Data of the Common Research Model with Natural Laminar Flow," *AIAA Scitech Forum 2021*, 2021. https://doi.org/10.2514/6.2021-1431.

[12] Qiao, L., Bai, J.-Q., adn Jing-Lei Xu, J.-K. X., and Zhang, Y., "Toward a Practical Method for Hypersonic Transition Prediction Based on Stability Correlations," *International Journal of Nonlinear Sciences adn Numerical Simulation*, Vol. 47, No. 10, 2018. https://doi.org/10.1515/ijnsns-2017-0011.

[13] Hao, Z., Yan, C., Qin, Y., and Zhou, L., "Improved $\gamma$-$\mathrm{Re}_{\Theta t}$ model for heat transfer prediction of hypersonic boundary layer transition," *International Journal of Heat and Mass Transfer*, Vol. 107, 2017. https://doi.org/10.1016/j.ijheatmasstransfer.2016.11.052.

[14] Ingen, J. L. V., "A Suggested Semi-Empirical Method for the Calculation of Boundary Layer Transition Region," *Delf University of Technology, Report No. VTH-74, Delft, the Netherlands*, 1956.

[15] Hildebrand, N., Chang, C.-L., Choudhari, M. M., Li, F., Nielsen, E., Venkatachari, B. S., and Paredes, P., "Coupling of the FUN3D Unstructured Flow Solver to the LASTRAC Stability Code to Model Transition," *AIAA Scitech Forum 2022*, 2022. https://doi.org/10.2514/6.2022-1952.

[16] Perraud, J., Arnal, D., Casalis, G., Archambaud, J. P., and Donelli, R., "Automatic Transition Predictions Using Simplified Methods," *AIAA Journal*, Vol. 47, No. 11, 2009, pp. 2676 – 2684.

[17] Krumbien, A., Krimmelbien, N., and Schrauf, G., "Automatic Transition Prediction in a Hybrid Flow Solver - Part 1: Methodology and Sensitivities," *Journal of Aircraft*, Vol. 46, No. 11, 2009, pp. 1176 – 1190.

[18] Krumbien, A., Krimmelbien, N., and Grabe, C., "Streamline-Based Transition Prediction Techniques in an Unstructured Computational Fluid Dynamics Code," *AIAA Journal*, Vol. 55, No. 5, 2017, pp. 1176 – 1190.

[19] Shi, Y., Mader, C., He, S., Halila, G. L. O., and Martins, J. R. R. A., "Natural Laminar-Flow Airfoil Optimizaton Design Using a Discrete Adjoint Approach," *AIAA Journal*, Vol. 58, No. 11, 2020, pp. 4702–4722.

[20] Halila, G. L. O., Fidkowski, K. J., and Martins, J. R. R. A., "Toward Automatic Parabolized Stability Equation-Based Transition-to-Turbulence Prediction for Aerodynamic Flows," *AIAA Journal*, Vol. 59, No. 2, 2020, pp. 462–473.

[21] Venkatachari, B. S., Carnes, J. A., Chang, C.-L., and Choudhari, M., "Boundary-Layer Transition Prediction Through Loose Coupling of OVERFLOW and LASTRAC," *AIAA Aviation Forum 2022*, American Institute of Aeronautics and Astronautics, 2022.

[22] Chang, C.-L., "LASTRAC.3d: Transition Prediction in 3D Boundary Layers," *34th Fluid Dynamics Conference and Exhibit*, American Institute of Aeronautics and Astronautics, 2004.

[23] Chang, C.-L., Kline, H., and Wang, X., *Langley Stability and Transition Analysis Code (LASTRAC) Version 3.0 User Manual*, NASA Langley Research Center, Hampton, VA, January 2022.

[24] Nichols, R. H., and Buning, P. G., *User's Manual for OVERFLOW 2.3*, NASA Langley Research Center, Hampton, VA, August 2010.

[25] Kimmel, R. L., Adamczak, D., Paull, A., Paull, R., Shannon, J., adn Myles Frost, R. P., and Alesi, H., "HIFiRE-1 Ascent-Phase Boundary-Layer Tranition," *Journal of Spacecraft and Rockets*, Vol. 52, No. 1, 2015. https://doi.org/10.2514/1.A32851.

[26] Li, F., Choudhari, M., Chang, C.-L., Kimmel, R., Adamczak, D., and Smith, M., "Transition Analysis for the Ascent Phase of HIFiRE-1 Flight Experiment," *Journal of Spacecraft and Rockets*, Vol. 52, No. 2, 2015, pp. 1283 – 1293. https://doi.org/10.2514/1.A33258.

[27] Paredes, P., Venkatachari, B., Choudhari, M. M., Li, F., Chang, C.-L., Zafar, M. I., and Xiao, H., "Toward a Practical Method for Hypersonic Transition Prediction Based on Stability Correlations," *AIAA Journal*, Vol. 58, No. 10, 2020, pp. 4475 – 4484. https://doi.org/10.2514/1.J05907.

[28] Horvath, T. J., Berry, S. A., Hollis, B. R., Chang, C.-L., and Singer, B. A., "Boundary Layer Transition on Slender Cones in Conventional and Low Disturbance Mach 6 Wind Tunnels," *32nd Fluid Dynamics Conference and Exhibit*, American Institute of Aeronautics and Astronautics, 2002.

[29] Tokugawa, N., Choudhari, M., Ueda, Y., Fujii, K., Atobe, T., Li, F., Chang, C.-L., and White, J., "Pressure Gradient Effects on Supersonic Transition over Axisymmetric Bodies at Incidence," *AIAA Journal*, Vol. 53, No. 12, 2015.

[30] Chen, F.-J., Malik, M. R., and Beckwith, I. E., "Boundary-Layer Transition on a Cone and Flat Plate at Mach 3.5," *AIAA Journal*, Vol. 27, No. 6, 1989.

[31] Malik, M. R., "Instability and Transition in Supersonic Boundary Layers," *Energy Resources Technology Conference*, American Society of Mechanical Engineers, 1984, pp. 139–147.

[32] Spallart, P. R., and Allmaras, S. R., "A One-Equation Turbulence Model for Aerodynamic Flows," *Recherche Aerospatiale*, Vol. 1, 1994, pp. 5 –21.

[33] Menter, F., Kuntz, M., and Langtry, R. B., "Ten Years of Industrial Experience with the SST Turbulence Model," *Journal of Heat and Mass Transfer*, Vol. 4, 2003.

[34] Chang, C.-L., "Development of Physics-Based Transition Models for Unstructured-Mesh CFD Codes Using Deep Learning Models," *AIAA Aviation Forum 2021*, 2021. https://doi.org/10.2514/6.2021-2828.

[35] Liu, Z., Lu, Y., Li, J., and Yan, C., "Local Correlation-Based Transition Model for High-Speed Flows," *AIAA Journal*, Vol. 60, 2022. https://doi.org/10.2514/1.J060994.

[36] Choudhari, M., Tokugawa, N., Li, F., Chang, C.-L., White, J. A., Ishikawa, H., Ueda, Y., Atobe, T., and Fujii, K., "Computational Investigation of Supersonic Boundary Layer Transition over Canonical Fuselage Nose Configurations," *7th Internation Conference on Computational Fluid Dyanmics*, 2012.